PERGAMON

Journal of Structural Geology 25 (2003) 481–501

JOURNAL OF STRUCTURAL GEOLOGY

www.elsevier.com/locate/jstrugeo

The Tellnes ilmenite deposit (Rogaland, South Norway): magnetic and petrofabric evidence for emplacement of a Ti-enriched noritic crystal mush in a fracture zone

Hervé Diot[a,*], Olivier Bolle[b,1], Jean-Marc Lambert[b], Patrick Launeau[c], Jean-Clair Duchesne[b]

[a]*Université de La Rochelle, Av. M. Crépeau, F-17042 La Rochelle Cedex 01, France*
[b]*Université de Liège, Bd. du Rectorat, Bât. B20, B-4000 Sart Tilman, Belgium*
[c]*Université de Nantes, 2 rue de la Houssinière, BP 92208, F-44322 Nantes, France*

Received 7 August 2001; accepted 21 December 2001

Abstract

The Tellnes ilmenite deposit, a world class titanium deposit, occurs in the Åna–Sira anorthosite (Rogaland anorthosite province, South Norway). It is mainly made up of an ilmenite-rich norite that has been previously interpreted as injected in a crystal mush state, in a weakness zone of the enclosing anorthosite. This emplacement mechanism has produced a faint orientation in the ore due to the flow of the mush. The internal flow structure of the orebody is studied here using the low-field anisotropy of magnetic susceptibility (AMS) method. Partial anhysteretic remanent magnetization (pAARM) indicates that coarse magnetite is the main mineral responsible for the magnetic fabric. Parallelism of the magnetic fabric with the shape-preferred orientation of the ore-forming minerals is checked using image analysis (IA) from oriented sections (intercept method). Interpretation of the AMS data verified by pAARM and IA, provides information on the magmatic foliation and lineation. Emplacement flow of the ilmenite norite crystal mush occurred in the direction of the orebody, parallel to its walls, and with an average SE 18° plunge. The feeder zone was likely situated below a network of veins on the SE end of the orebody. The sickle-shaped outcrop of the deposit suggests a transcurrent, dextral opening of a WNW–ESE-striking weakness zone across the anorthosite pluton.

Keywords: Titanium deposit; Petrofabric; Anisotropy of magnetic susceptibility (AMS); Rogaland, Norway

1. Introduction

The Tellnes ilmenite deposit (TID) (Sokndal district, Rogaland, South Norway) is the largest Ti–Fe orebody in Europe, and the second most important ilmenite orebody in production in the world today, just after Lake Tio deposit (Allard Lake district, Quebec). In 1999, its yearly production was 550,000 tons of ilmenite concentrate, averaging 44.5% TiO_2, and represented 5% of the world's TiO_2 production (Titania A/S, pers. comm. 1999). The TID is a hard-rock orebody of igneous origin, which consists of an ilmenite norite lens emplaced in the Rogaland anorthosite province (e.g. Duchesne et al., 1985), an AMC (anorthosite–mangerite–charnockite)[2] igneous complex of Late-Proterozoic age, characterized by huge anorthosite bodies (Krause and Pedall, 1980; Krause et al., 1985; Duchesne, 1999). Ilmenite and magnetite magmatic deposits of subeconomic to economic grade are widespread in this area but Tellnes is today the largest and richest deposit (Force, 1991). The Rogaland anorthosite province is part of the Sveconorwegian orogenic province, correlated with the Greenville province in North America. In sharp contrast to many North American occurrences, however, the Rogaland anorthosites and associated Ti–Fe deposits were emplaced during a post-collisional magmatic activity period (Schärer et al., 1996; Duchesne et al., 1999). The Rogaland Ti–Fe deposits thus escaped regional tectonic reworking and metamorphism, even if most of them crystallized or recrystallized during syn-plutonic deformation of the diapirically emplaced anorthosites (Duchesne et al., 1985;

* Corresponding author. Tel.: +33-5-46-45-86-18; fax: +33-5-46-45-86-18.
E-mail address: hdiot@univ-lr.fr (H. Diot).
[1] Post-doctoral Researcher from the Belgian F.N.R.S. (National Fund for Scientific Research, Belgium).
[2] Nomenclature of the AMC rocks is (Streckeisen, 1974): anorthosite = rock with plagioclase content >90%; (leuco)(mela) norite = hypersthene (leuco)(mela)gabbro; jotunite = hypersthene monzogabbro; (quartz) mangerite = hypersthene (quartz) monzonite; charnockite = hypersthene granite.

0191-8141/03/$ - see front matter © 2002 Elsevier Science Ltd. All rights reserved.
PII: S0191-8141(02)00050-0

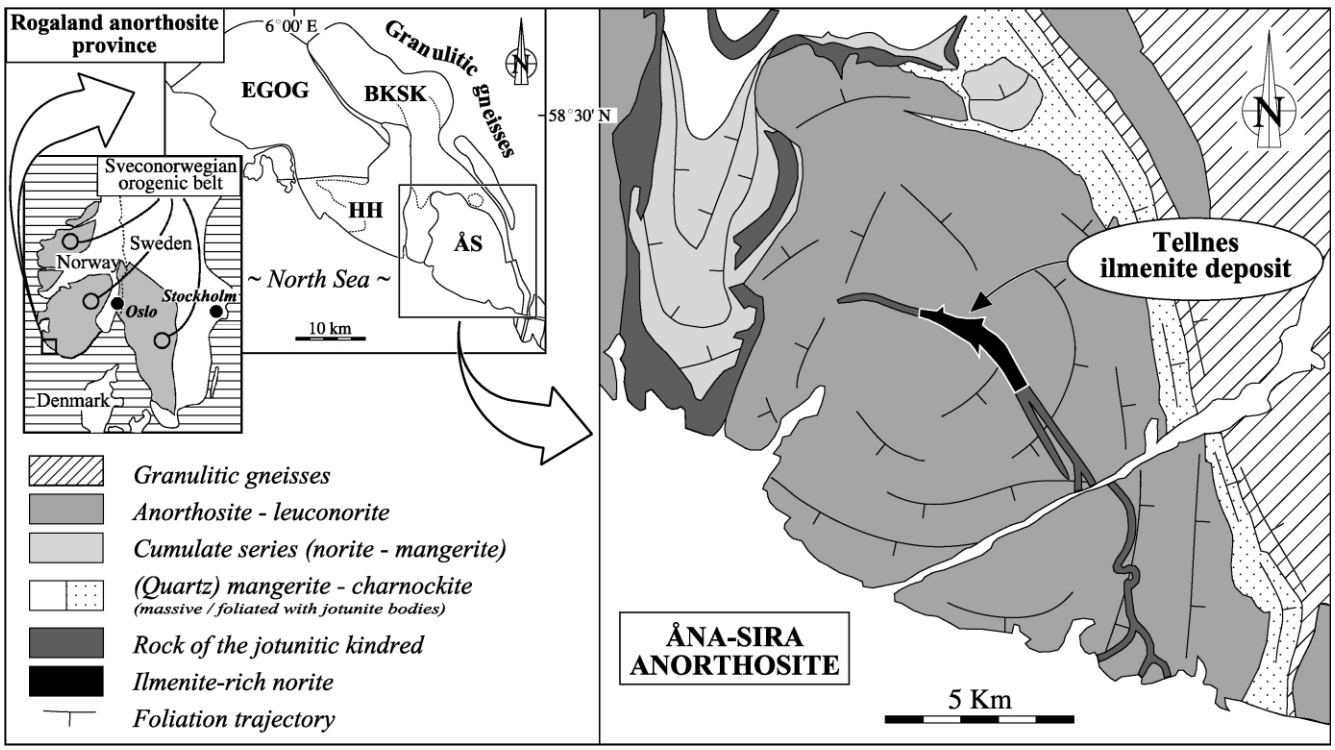

Fig. 1. Geological sketch map of the Rogaland anorthosite province (modified from Duchesne et al., 1985) (EGOG, HH, ÅS: Egersund–Ogna, Håland–Helleren, and Åna–Sira anorthosite bodies, respectively; BKSK: Bjerkreim–Sokndal intrusion), with detailed geology of the Åna–Sira anorthosite (modified from Krause and Pedall, 1980; Krause et al., 1985) and location in the Sveconorwegian orogenic belt.

Barnichon et al., 1999). The TID is an exception among the Rogaland Ti–Fe deposits: being related to a late structure, it has not been affected by anorthosite emplacement (Duchesne, 1999; Duchesne and Schiellerup, 2001). It thus provides a special opportunity to study genetic and structural primary relationships between anorthosites and ilmenite deposits.

The TID has been extensively studied, on the basis of field, petrographical and geochemical data (e.g. Gierth, 1970; Gierth and Krause, 1973; Krause and Pedall, 1980; Krause et al., 1985; Wilmart et al., 1989; Duchesne, 1999), which led to a detailed knowledge of the mineralization. Despite these numerous studies, the internal structure of the TID was, up to now, poorly constrained, because of the ill-defined aspect of the petrofabric. The present paper proposes such a scenario, deduced from a thorough structural study using the low-field anisotropy of magnetic susceptibility (AMS) method (e.g. Rochette et al., 1992; Borradaile and Henry, 1997), a fast and efficient structural method, now widely used for fabric determination in weakly anisotropic rocks (mainly granitoids, see e.g. Bouchez, 1997). AMS is here complemented by an image analysis (IA) investigation (based on the intercept method of Launeau and Robin (1996)) and by some anisotropy of partial anhysteretic remanent magnetization (pAARM) measurements (Jackson et al., 1988; Trindade et al., 2001), in order to validate the AMS results (i.e. to check parallelism between magnetic fabric and petrofabric) and to investigate mineral sources that carry AMS.

This is the first application of the AMS method to a Ti–Fe mineralization of major economic interest. Combined with other structural approaches (IA, pAARM), it provides a model that sheds new light on the emplacement and enrichment mechanisms of ilmenite igneous orebodies associated with an anorthosite complexes.

2. Geological setting

2.1. The Rogaland anorthosite province

The Rogaland anorthosite province (see e.g. Duchesne et al. (1985) for a review) outcrops in the southwestern part of the Sveconorwegian orogenic belt (Fig. 1), in various ortho- and paragneiss complexes that were metamorphosed in the granulite facies (e.g. Falkum and Petersen, 1980). The North Sea covers about 70% of the igneous complex. The main geological units recognized on-shore (Fig. 1) are three anorthosite plutons (the Egersund–Ogna, Håland–Helleren and Åna–Sira bodies) and the Bjerkreim–Sokndal intrusion, a folded layered body which exhibits a thick series of anorthosite–(leuco)norite–mangerite cumulates capped by massive acidic rocks (quartz mangerite and charnockite). Minor components of the Rogaland anorthosite province

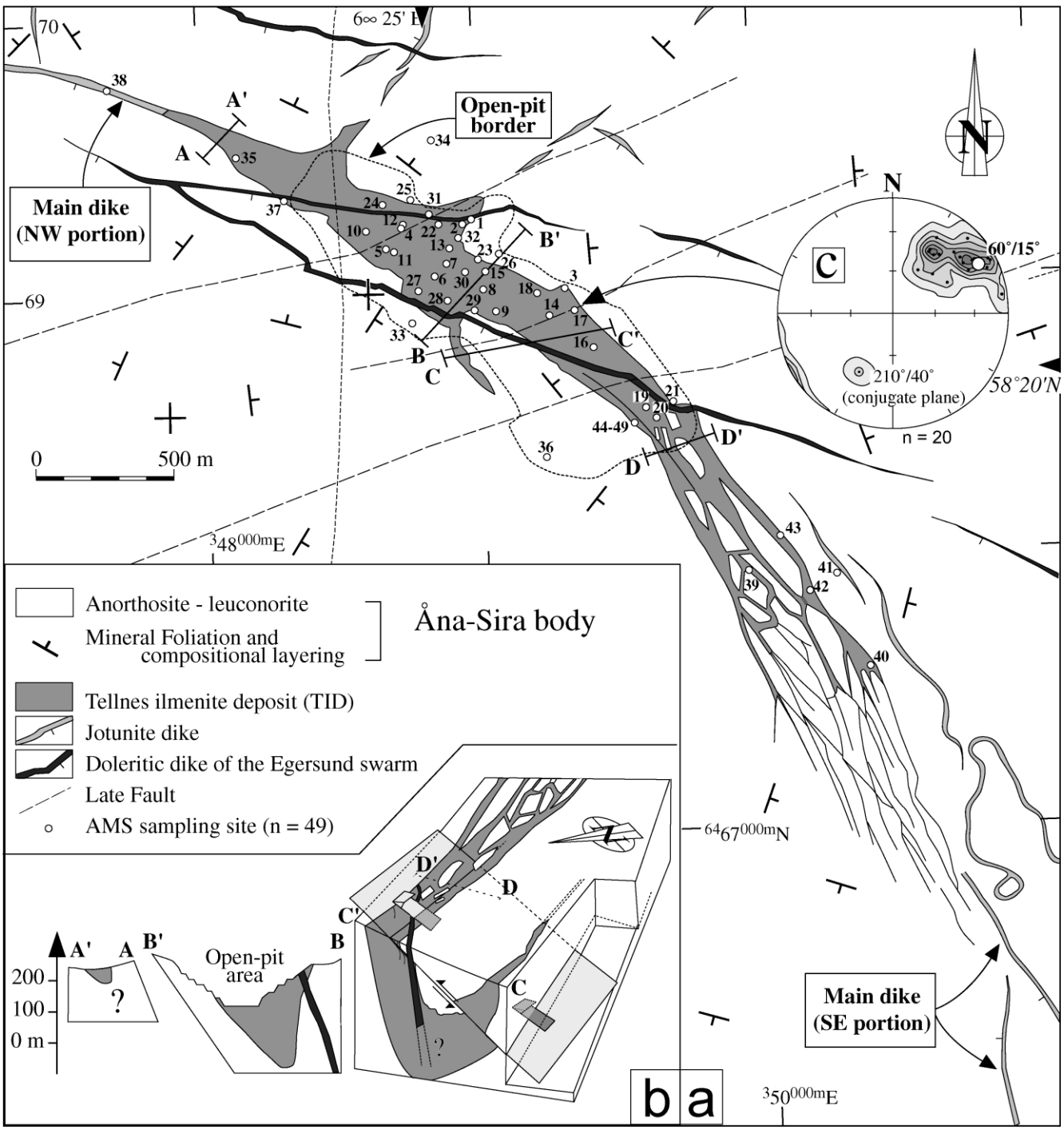

Fig. 2. (a) Geological map of the TID (Krause and Pedall, 1980; Krause et al., 1985; Karlsen et al., 1998; E. Gierth, pers. comm., 2000; Titania A/S pers. comm. of K. Berge and R. Hagen, 2000). Grid is the EURF89 kilometric UTM. (b) Schematic cross-sections in the orebody (see location of profiles in (a)). (c) Schmidt stereo-plot (lower hemisphere) with poles of early/late extension fractures.

include: (1) two leuconorite outliers, outcropping along the eastern border of the complex; (2) dikes and small jotunitic plutons that cut across the anorthosite bodies and the cumulate series of the Bjerkreim–Sokndal intrusion; and (3) numerous Ti–Fe deposits, which are mainly found in the Håland–Helleren and Åna–Sira anorthosites.

Zircon and baddeleyite U–Pb ages indicate that the whole Rogaland anorthosite province was emplaced in a very short time interval, between ~930 and 920 Ma (Schärer et al., 1996, and references therein). In agreement with the anorthosite model (Ashwal, 1993), the three Rogaland anorthosite plutons are interpreted to result from the diapiric emplacement of a plagioclase crystal mush, which crystallized over a large P–T interval, from a deep-seated magma chamber (at 11–13 kbar) up to mid-crustal depth (around 5 kbar) (Duchesne et al., 1985; Longhi et al.,

Table 1
Average modal proportion and chemical composition of the ore forming minerals in the TID. References: (a) Gierth (1970); (b) Duchesne (1973); (c) Gierth and Krause (1973); (d) Wilmart et al. (1989); (e) Duchesne (1999)

Ore forming minerals	Modal proportion (vol. %) (a)	Chemical composition
Plagioclase	53.2	An45–42 (d)
Hemo-ilmenite	28.6	Hem13–15 (b, e)
Orthopyroxene	10.2	En77–75 (bronzite) (d)
Biotite	3.9	Ti-rich (c)
Magnetite	0.7–2.5	Usp2.5–3, Cr–V–Zn rich (b, e)
Olivine, apatite, Fe–Ni–(Co)–Cu sulfides, clinopyroxene and other accessories	3.4	Olivine is Fo80 (d)

1999). The syncline shape of the neighboring Bjerkreim–Sokndal intrusion has been interpreted as resulting from a gravity-induced subsidence, probably coeval with, and possibly triggered by, the final emplacement and coalescence of the anorthosite plutons (Bolle et al., 2000). Gravity instabilities can therefore account for both the emplacement and deformation of the Rogaland anorthosite province main volume. A crustal weakness zone may, however, have channeled emplacement and ascent of the anorthosites (Duchesne et al., 1999).

2.2. The Tellnes ilmenite deposit

The TID outcrops in the central part of the Åna–Sira anorthosite (Krause and Pedall, 1980; Krause et al., 1985), the easternmost Rogaland anorthosite pluton (Fig. 1). This ~200 km^2 anorthosite pluton is mainly made up of coarse-grained anorthosite, and also comprises more leuconoritic parts, as well as anorthosito–leuconoritic complexes (i.e. lenses or patches of norite or leuconorite embedded into anorthosite, or inversely). It is dome-shaped and geophysical data (gravity measurements) suggest a minimum thickness of about 4 km (Smithson and Ramberg, 1979). U–Pb dates from zircons give an age of 932 ± 3 Ma for the Åna–Sira anorthosite (Schärer et al., 1996).

From detailed geological mapping (Krause and Pedall, 1980; Krause et al., 1985) and mining prospecting, it appears that: (1) the TID has a WNW–ESE to NNW–SSE sickle-shaped outcrop trend, is greater than 400 m wide in its central part and is greater than 2700 m long; and (2) the 3D shape of the TID is that of a SE-plunging elongated trough, whose NE and SW flanks dip, respectively, SW 45–50° and from almost vertical to NE, and which ends south-eastwards in an ill-defined dike-like unit (Fig. 2a and b). Sharp contacts, apophyses injected into the host rocks, intrusive breccias, and anorthosite xenoliths (especially abundant in the TID south-eastern end) are evidence for the intrusive character of the orebody (e.g. Krause et al., 1985).

Joints, faults and lineaments are numerous across the TID and the surrounding anorthosite, and they often have guided weathering fluids (Karlsen et al., 1998). A weakly-spaced, incipient cleavage is particularly well developed in the orebody itself, especially in its south-eastern and north-western ends and in the adjacent anorthosite. This dense cleavage is sub-vertical and strikes parallel to the contacts of the TID, i.e. WNW–ESE to the NW and NNW–SSE to the SE. In the absence of any evidence of relative movement along these joints, they are interpreted as resulting from a tensile stress during emplacement of the TID. Both experimental (Hoagland et al., 1973; Pollard, 1973) and field (Delaney et al., 1986) work describe a close relationship between dike emplacement and joint formation. On a larger scale, a NW–SE-trending and SW-dipping, reverse ductile fault is observed at the SE end of the open-pit, locally reactivating the SW flank of the TID, which actually reduces the thickness of the mineralization in that area (Fig. 2a and b). Moreover, major post-mineralization, usually WSW–ENE striking, faults that intersect the TID (Fig. 2a) cause an overall vertical displacement of the orebody of about 80–100 m (Krause et al., 1985). Two sub-vertical, WNW–ESE striking, doleritic dikes also intersect the orebody (Fig. 2a and b). They belong to the Egersund doleritic dike swarm (dated to 616 ± 3 Ma; baddeleyite U–Pb age of Bingen et al. (1998)), that cut across the whole Rogaland anorthosite province and the surrounding high-grade terranes.

The dominant petrographic facies in the TID (Gierth and Krause, 1973; Wilmart et al., 1989) is a medium-grained ilmenite-rich norite, mainly made up of plagioclase, hemo-ilmenite and orthopyroxene, with subordinate biotite, magnetite, olivine, apatite, and at least 22 other accessory minerals in minor to trace amounts (including complex Fe–Ni–(Co)–Cu sulfides and clinopyroxene) (Table 1). The cumulate character of this association (substantiated for the plagioclase) by a distinct positive Eu anomaly in the whole-rock REE distributions (Wilmart et al., 1989), is generally accepted (Duchesne and Schiellerup, 2001). Slight and progressive variations in the modal proportion and chemical composition of the ore-forming minerals are observed, from the central part towards the contacts of the orebody (Krause et al., 1985; Wilmart et al., 1989; Duchesne and Schiellerup, 2001): the most obvious modifications are an increase of the plagioclase content and a decrease of the ilmenite one, and a reduction of the plagioclase An content and orthopyroxene Mg# (from 45–42 to 39 and 0.77 to 0.60, respectively; Wilmart et al., 1989). These variations give rise, along the orebody flanks, to more leucocratic rocks (i.e. more plagioclase-rich and ilmenite-poor), of non or lower

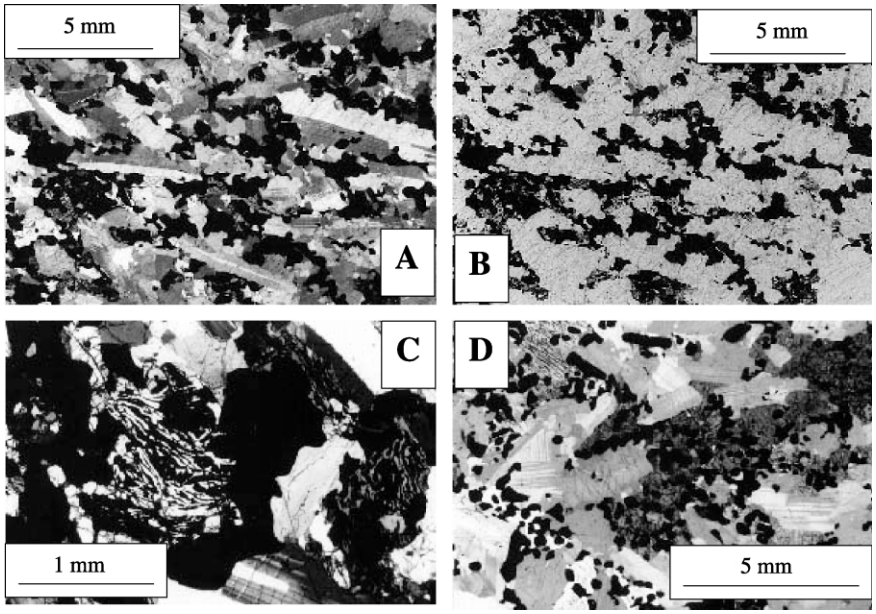

Fig. 3. Photomicrographs of ilmenite-rich norite samples from the TID. (a) Sample T13, slightly crossed nicols; and (b) same sample, uncrossed nicols. Elongated euhedral plagioclase crystals (with Carlsbad and albite twinning) form a framework and the interstices of which are filled with smaller ilmenite, pyroxene and biotite grains. The opaque grain fabric define an approximate 'negative' image of this framework and mimics the petrofabric (also (d)). Rare inclusions of sub-spherical ilmenite grains in plagioclase. (c) Sample T2, crossed nicols. Symplectitic intergrowths of magnetite and orthopyroxene (formed by olivine destabilization). (d) Sample T17, slightly uncrossed nicols. A large poikilitic orthopyroxene crystal develops in the interstices of a framework of plagioclase and includes sub-spherical ilmenite grains.

economical interest, which are also found in some apophyses and in the south-eastern end of the TID. Two petrogenetic models have been proposed to explain these mineralogical variations: (1) in-situ crystallization of a noritic magma, inward from the orebody flanks (Krause and Pedall, 1980; Krause et al., 1985; Force, 1991); and (2) injection of crystal-rich mush batches, lubricated by a few percent of interstitial liquid, coming from a neighboring magma chamber. This adjacent magma chamber had a zoned cumulate pile, enriched in dense Ti–Fe minerals at the base and in light plagioclases at the top, and had developed by (gravity) fractional crystallization (Wilmart et al., 1989). The latter model is based on the observation that ilmenite-rich norites and more leucocratic rocks from the TID plot on mixing linear trends in variation diagrams of major element contents. The absence of gravity-induced zoning involves an already large ($35\% < \%\text{Crystals} < 70\%$) crystallization with a Bingham type behavior for the crystal mush. The only vertical mineralogical variation in the TID concerns the magnetite and sulfide contents (Force, 1991; Duchesne and Schiellerup, 2001). The orebody can be divided into an upper part, showing relatively high magnetite content (1–3 wt.%) and abundant sulfides (>2500 ppm), and a lower part, with almost no magnetite and sulfides. All these variations in the modal contents of the ore-forming minerals are reflected through subtle variations in the ore geochemistry (Duchesne and Schiellerup, 2001).

Towards the north-west and the south-east, the TID is geometrically connected to one of the jotunitic dikes that cut across the Rogaland anorthosite province: the Tellnes main dike (Wilmart et al., 1989) (Figs. 1 and 2). To the north-west, this dike has a WNW–ESE-trend and is more than 4 km long. To the south-east, it runs for more than 10 km, with a NNW–SSE orientation changing southwards to a N–S one. The thickness varies from 5 to 10 m. The texture is medium- to fine-grained and the composition ranges from a jotunite to a quartz mangerite (Wilmart et al., 1989). To explain the close association of ilmenite norite and more evolved products of intermediate to acidic composition in the same geological unit, Krause and Pedall (1980) advanced the thesis of a single intrusion which differentiated laterally into both the TID and the main dike. Sr isotopes and geochemical modeling show, however, that the TID and the main dike are not co-magmatic (Wilmart et al., 1989). Moreover Schärer et al. (1996) measured a 10 Myr difference in age between the main dike (931 ± 5 Ma) and the TID (920 ± 3 Ma). Moreover, we have observed a strong deformation in the main dike (dynamic recrystallization of the plagioclase, pull-apart of pyroxene along the lineation) near its NW connection with the TID, which could be related to the emplacement of this latter.

3. Sample description and magnetic mineralogy

The samples used in the present study consist of 25-mm-diameter oriented cores, collected with a portable drilling machine, and oriented blocks. They come from 49 sites, essentially located inside the open-pit (Fig. 2a). The main

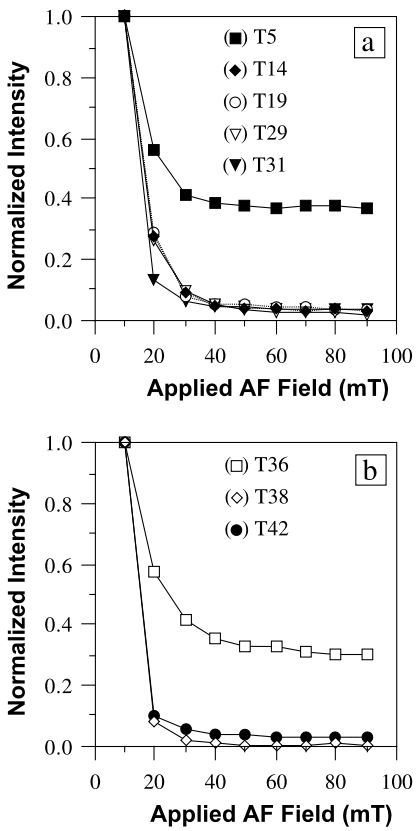

Fig. 4. Normalized coercivity spectra of specimens from selected AMS sites in: (a) the open-pit (ore samples; T5, T14, T19, T29, T31); and (b) the south-eastern end of the orebody (T42), the main dike (T38) and the Åna–Sira anorthosite (T36). Each 10 mT interval in the abscissa corresponds to the windows of AF during DC field application of 0.05 mT.

facies sampled in the TID is the ore, i.e. ilmenite-rich (mela)norite. Plagioclase-enriched varieties were also collected along the contact of the orebody, in its south-eastern and north-western ends, and in apophyses (nine sites; T1, T23, T32, T35, T40, T42, T43, T44, T49). Some samples were also collected in the Åna–Sira anorthosite (seven sites; T21, T25, T26, T33, T34, T36, T41) and in the main dike (a single site; T38) for the sake of comparison. A petrographical description of the magnetic mineralogy, based on a reflected- and transmitted-light microscopic study, is presented below.

In the ore and its plagioclase-enriched varieties, the paramagnetic minerals are ilmenite and orthopyroxene, accessory biotite flakes (ubiquitous) and olivine grains (in some samples). Clinopyroxene is also present as external exsolution granules at the border of orthopyroxene grains and also as primary grains, mostly in samples collected near the contact of the orebody, and in its south-eastern and north-western ends). Orthopyroxene and primary clinopyroxene usually contain opaque, ultra-thin Schiller-type exsolutions, in one or two crystallographic planes. These exsolutions are made up of ilmenite and hemo-ilmenite or, exceptionally, magnetite. Ilmenite grains show multiple generations of abundant, fine hematite exsolution lenses and rare aluminous spinel needle-like exsolutions. Accessory magnetite is also present in many samples, as grains (usually some tens to several hundreds of micrometers large) that contain exsolutions of aluminous spinel (also found as external granules). Where magnetite and ilmenite grains are in contact, a thin reaction rim of spinelliferous ilmenite (magnetite–spinel–ilmenite symplectite) has developed at the ilmenite–magnetite grain boundary and, close to this rim, hematite exsolutions in the ilmenite have disappeared. Both microtextures reflect subsolidus reequilibration (diffusion) between the two oxides (Duchesne, 1973). Magnetite can also form symplectitic intergrowths with orthopyroxene (Fig. 3c), resulting from olivine destabilization (Gierth and Krause, 1973). Minor to trace amounts of sulfide grains (bravoite, chalcopyrite, covellite, marcassite, millerite, pentlandite, pyrite, pyrrhotite, siegenite and violarite; Gierth et al., 1982), observed in all samples may also play a minor role in the magnetic mineralogy. Ubiquitous microfractures, filled with an opaque phase (ilmenite, magnetite or/and sulfide) may also contribute to the bulk magnetic signature. These microfractures are probably coeval with weathering processes, evidenced in many samples by, (1) a low-T transformation of orthopyroxene, olivine and locally, biotite and, (2) the presence of thin fractures coated with secondary chlorite fibers. Regarding the abundance of para- and ferromagnetic minerals, the role of the diamagnetic minerals (plagioclase and minor apatite) can be neglected.

The sample from the main dike (T38) shows a mosaic of diamagnetic minerals (plagioclase, minor potassium feldspar) and some clinopyroxene, in which orthopyroxene (inverted pigeonite) develops poikilitic crystals. Homogeneous grains of ilmenite and magnetite are found as accessories, and traces of Fe–Cu sulfides are observed.

In the samples coming from the Åna–Sira anorthosite, orthopyroxene (often with hemo-ilmenite, Schiller-type exsolutions), clinopyroxene and biotite are found. Minor to trace minerals occur in the interstices between plagioclase crystals that contain minute needles of rutile and oxide (hematite or magnetite?). Trace amounts of small opaque grains (a few tens of micrometers) are also observed, including hemo-ilmenite and some ilmeno-hematite, magnetite, and Fe–Cu sulfides.

The magnetic mineralogy of the samples is therefore very complex, with various para- and ferromagnetic minerals that may contribute to the magnetic mineralogy, according to their respective modal proportions and intrinsic magnetic properties (Jackson, 1991; Borradaile and Henry, 1997). The existence of para- and ferromagnetic exsolutions and inclusions in dia- and paramagnetic grains is another complicating factor (e.g. Lagroix and Borradaile, 2000).

Additional information on the ferromagnetic mineralogy were obtained for representative samples by determination of coercivity spectra on individual rock cylinders (25 mm × 22 mm), cut from the 25-mm-diameter drilled cores (Fig. 4a and b; see Appendix A for methodology).

The coercivity spectra all exhibit a similar shape (Fig. 4a

Table 2
AMS data. X, Y = coordinates in the EURF89 kilometric UTM grid (32 V zone, LK 100 km square) and Z = altitude. N: number of individual specimens measured per site; K_m: magnitude of the bulk magnetic susceptibility (see text for definition); P' and T: anisotropy degree and shape parameters of Jelinek (1981) (see text for definition); K_1 and K_3: long and short principal axes of the AMS ellipsoid; Dec. and Inc.: declination and inclination of the axes; s_1 and s_2: semiangle of the major and minor axes of a 3σ confidence ellipse

Site	X (km)	Y (km)	Z (m)	N	K_m (10^{-3} SI)	P'	T	K_1				K_3				Petro-graphic type
								Dec.	Inc.	s_1	s_2	Dec.	Inc.	s_1	s_2	
T1	48.950	69.240	205	6	7.8	1.15	−0.20	170	25	61	39	267	14	66	45	L
T2	48.900	69.230	190	6	20.8	1.12	0.22	187	15	64	17	279	6	36	12	IN
T3	49.280	68.990	155	5	82.4	1.01	0.00	153	32	69	17	267	33	72	12	IM
T4	48.690	69.220	100	5	3.7	1.04	0.00	147	14	23	8	246	34	40	5	IN
T5	48.630	69.150	100	5	8.3	1.11	−0.07	328	2	57	15	236	41	39	8	IN
T6	48.810	69.040	95	4	24.8	1.15	−0.42	159	8	14	12	282	75	44	8	IN
T7	48.850	69.090	95	6	25.1	1.21	−0.64	151	3	15	11	243	32	35	11	IN
T8	48.980	68.990	100	6	34.3	1.11	0.09	151	19	16	10	279	61	14	11	IN
T9	49.030	68.910	110	4	35.9	1.12	−0.03	128	13	40	10	234	50	30	10	IN
T10	48.560	69.220	120	5	7.5	1.04	0.47	12	54	47	29	261	15	46	11	IM
T11	48.660	69.140	110	6	8.4	1.09	0.30	345	14	54	11	246	34	37	14	IN
T12	48.700	69.240	110	6	5.4	1.09	0.18	195	35	50	23	5	54	35	14	IN
T13	48.860	69.140	110	6	26.2	1.13	−0.09	178	40	41	23	69	21	37	28	IN
T14	49.220	68.890	115	5	47.1	1.17	0.01	169	24	32	15	350	66	28	12	IN
T15	48.990	69.060	110	6	30.9	1.18	0.21	149	27	20	2	43	29	25	2	IN
T16	49.370	68.770	135	4	57.8	1.14	0.43	176	9	37	12	311	77	35	6	IN
T17	49.310	68.900	130	4	40.4	1.08	−0.17	170	3	102	47	70	76	96	56	IN
T18	49.180	68.970	125	5	11.7	1.19	−0.77	177	26	26	7	73	28	90	8	IN
T19	49.560	68.540	165	5	16.5	1.09	−0.09	330	1	42	23	61	32	38	29	IN
T20	49.600	68.500	175	4	38.2	1.06	−0.42	149	0	18	14	59	47	71	13	IN
T21	49.650	68.560	175	6	1.9	1.13	−0.31	127	55	72	29	295	35	102	39	A
T22	48.820	69.230	145	4	3.4	1.05	0.47	123	8	70	48	20	58	71	28	IN
T23	48.970	69.110	140	4	29.2	1.16	0.02	154	28	13	4	245	0	56	6	N
T24	48.630	69.310	175	5	23.3	1.24	0.25	142	32	58	21	26	35	36	19	IN
T25	48.730	69.330	210	3	1.3	1.17	−0.01	120	30	25	16	232	33	22	4	A
T26	49.040	69.120	175	6	1.9	1.10	0.06	99	51	76	26	245	34	79	35	A
T27	48.750	68.990	145	5	7.4	1.23	0.55	32	68	35	5	233	21	14	6	IN
T28	48.850	68.960	140	3	20.7	1.10	0.08	115	40	14	5	212	8	55	5	IN
T29	48.950	68.920	145	4	45.5	1.08	−0.17	107	59	48	11	203	4	39	6	IN
T30	48.920	69.060	100	6	40.0	1.10	0.30	155	46	35	14	49	15	30	11	IN
T31	48.790	69.270	175	5	42.5	1.02	−0.09	158	31	18	7	309	56	32	15	IN
T32	48.900	69.180	175	4	24.7	1.02	0.25	357	54	37	13	265	1	36	11	L
T33	48.720	68.880	215	4	1.5	1.32	−0.20	76	49	55	22	242	41	56	33	A
T34	48.810	69.540	305	4	0.5	1.24	−0.07	35	44	58	35	170	37	63	40	A
T35	48.100	69.500	260	6	6.8	1.10	0.48	143	15	86	17	240	25	65	9	L
T36	49.190	68.380	230	4	1.9	1.21	0.15	138	45	38	15	277	37	24	11	A
T37	48.270	69.330	235	4	3.1	1.01	0.00	332	15	23	12	84	54	42	11	IN
T38	47.640	69.760	250	4	56.7	1.05	0.16	311	17	28	11	47	19	30	7	FJ
T39	49.910	67.940	280	5	84.3	1.02	0.00	162	21	18	5	255	8	15	8	IM
T40	50.340	67.580	320	4	18.3	1.01	0.02	160	19	79	14	68	8	90	35	L

(*continued on next page*)

Table 2 (*continued*)

Site	*X* (km)	*Y* (km)	*Z* (m)	*N*	K_m (10^{-3} SI)	P'	*T*	K_1				K_3				Petro-graphic type
								Dec.	Inc.	s_1	s_2	Dec.	Inc.	s_1	s_2	
T41	50.230	67.920	280	5	0.4	1.13	−0.05	111	40	62	11	202	1	65	37	L
T42	50.130	67.860	280	4	23.4	1.08	0.56	153	26	43	13	250	14	29	3	L
T43	50.040	68.030	300	5	22.5	1.19	0.59	334	56	71	31	243	1	39	7	L
T44	49.510	68.480	190	4	14.1	1.25	0.18	173	7	19	9	271	48	30	8	L
T45	49.510	68.480	190	4	59.3	1.12	0.55	176	28	76	8	273	13	16	6	IN
T46	49.510	68.480	190	4	47.4	1.16	0.54	190	55	92	6	76	16	16	14	IN
T47	49.510	68.480	190	3	43.1	1.13	0.31	181	8	33	25	273	9	26	23	IN
T48	49.510	68.480	190	4	22.5	1.10	0.22	305	77	68	15	60	6	51	10	IN
T49	49.510	68.480	190	4	57.6	1.12	0.17	357	11	72	5	261	28	61	25	L

Petrographic type

	Olivine	Opx	Cpx	Biotite	Ilmenite	Magnetite: Symplec	Magnetite: Grains
L = Leuconorite		- - - - -	- -	- - -	- - - -	-	-
IN = Ilmenite-rich norite	-	- - - - -	-	- - -	- - - - -	- -	- - -
IM = Ilmenite-rich melanorite	- -	- - - - -	-	- - - -	- - - - -	-	- -
N = Norite		- - - - -	- -	- - - -	- - - - -		-
A = Anorthosite		-		-	-		-
FJ = Fine-grained jotunite		- - - -	- -	-	- -		- -

- - - - - = abundant
- - - - = common
- - - = frequent
- - = uncommon
- = traces

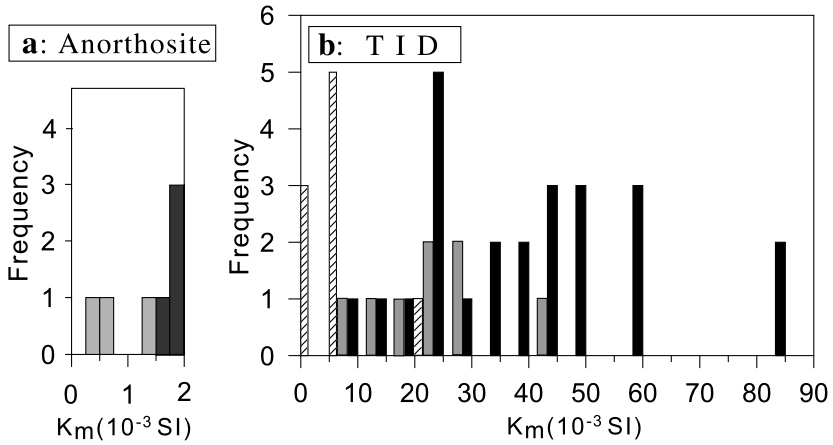

Fig. 5. Partial histograms of the bulk magnetic susceptibility (K_m) frequency for AMS samples: (a) from the Åna–Sira anorthosite, containing no magnetite (in gray shade), with traces of magnetite grains (in black shade); (b) from the TID, with no magnetite grains (clear gray shaded and striped), with large magnetite grains as trace minerals (medium gray shaded) and with minor amounts of large magnetite grains (black).

and b and Appendix A methodology). The peak value of the pARM at low AF magnetization values ((20 mT), followed by a smooth decrease, with increasing AF magnetization, down to the background remanent magnetization. The non-zero background results from the presence of hematite exsolutions in ilmenite, except in T38 in which ilmenite is devoid of exsolutions. Since coercivity is linked to grain size (Jackson et al., 1988; Jackson, 1991), the peak pARM can directly be correlated to the large, low-coercivity grains of magnetite present in the samples. For T5 (Fig. 4a) and T36 (Fig. 4b), the high value of the background remanent magnetization, relative to the peak one's, expresses the scarcity of the magnetite grains.

Moreover, it appears that the background is attained only for an AF magnetization value that varies, from one specimen to another, from 40 to 70 mT. This reveals a pARM due to small, medium-coercivity magnetite grains (<5 μm according to the magnetite coercivity vs. grain size data of Jackson et al. (1988) and Vlag et al. (1996)). Some small magnetite grains and symplectites, as well as the oxide fine exsolutions in orthopyroxene and plagioclase, and the oxide micro-fractures fall in this size range, which suggests a composite character for the medium-coercivity magnetite fraction.

4. Anisotropy of magnetic susceptibility

AMS was measured on a total of 230 rock cylinders (25 mm × 22 mm) cut from the 25-mm-diameter cores that were drilled at the 49 sampling sites (see Appendix A for methodology). The results of the measurements are given in Table 2.

4.1. Scalar parameters

The bulk magnetic susceptibility, $K_m = (K_1 + K_2 + K_3)/3$, varies from 0.4 to 1.9×10^{-3} SI in the Åna–Sira anorthosite (Table 2). These values do not significantly depart from the 10^{-3} SI limit defined by Rochette (1987), above which rock magnetic susceptibility is dominantly ferromagnetic. Hence, in the anorthosite samples, contributions to K_m from both the paramagnetic and ferromagnetic minerals have to be taken into account. K_m ranges from 0.4 to 1.3×10^{-3} SI for samples where magnetite was not optically observed and from 1.5 to 1.9×10^{-3} SI for samples containing traces of magnetite grains (Fig. 5a). This points to a relatively strong control of K_m by the magnetite grains when present.

In the main dike (T38), $K_m = 56.7 \times 10^{-3}$ and in the TID, K_m varies from 3.1 to 84.3×10^{-3} SI (Table 2). These values are high ($\geqslant 10^{-3}$ SI), which suggests a dominant ferromagnetic contribution to the bulk magnetic susceptibility (Rochette, 1987). In the main dike, it is reasonable to think that magnetite grains, the only ferromagnetic minerals, are the main magnetic susceptibility carriers. In the TID, when samples are considered according to their content of (large) magnetite grains, three overlapping frequency histograms can be distinguished: (1) for samples optically devoid of large magnetite grains, K_m varies from 3.1 to 20.8×10^{-3} SI (average of 7.6×10^{-3} SI) (Fig. 5b); (2) for samples with a few large magnetite grains, K_m is from 7.4 to 40.4×10^{-3} SI (average of 22.6×10^{-3} SI) (Fig. 5b); and (3) for samples with more abundant, but still minor, large magnetite grains, K_m ranges from 6.8 to 84.3×10^{-3} SI (average of 38.5×10^{-3} SI) (Fig. 5b). These frequency distributions suggest that the wide range of K_m values observed in the TID probably reflects equally wide variations in the content of large magnetite grains, and that contribution of this high-susceptibility mineral to K_m values is dominant in most samples. This conclusion is, however, probably partly distorted by: (1) the heterogeneous distribution of the accessory magnetite grains at the sample scale, which are missed by petrographical observations. For example, no large magnetite grain was optically detected in T5, when the coercivity spectrum indicates that a few of

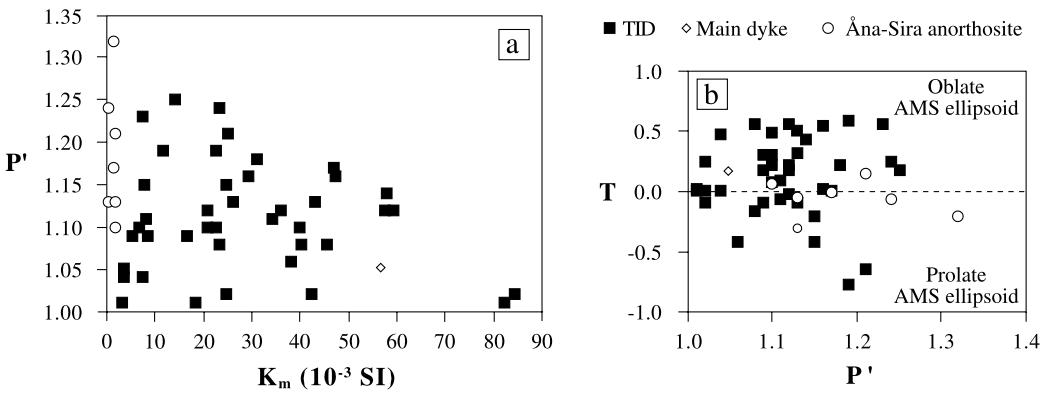

Fig. 6. (a) Plot of the AMS anisotropy degree of Jelinek (1981) (P') vs. bulk magnetic susceptibility (K_m); (b) Plot of the Jelinek (1981) AMS shape parameter (T) vs. anisotropy degree (P').

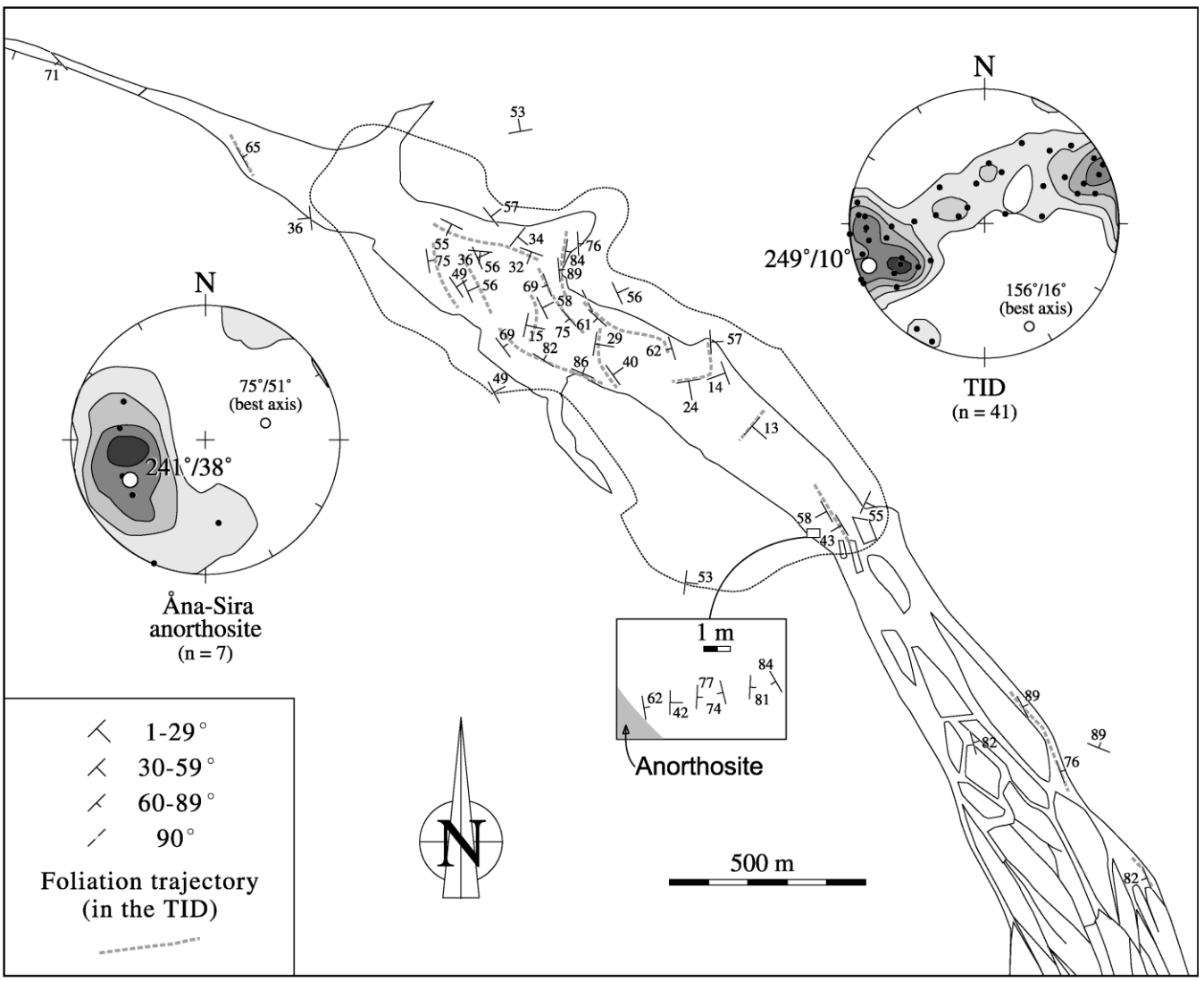

Fig. 7. Map of the magnetic foliations (perpendicular to K_3 axes), with Schmidt stereo-plot (lower hemisphere) of contours of the poles to these foliations with average value and best axis (pole of the best great circle of the distribution of the poles statically determined) for data in the TID and in the Åna–Sira anorthosite (n: number of measurements).

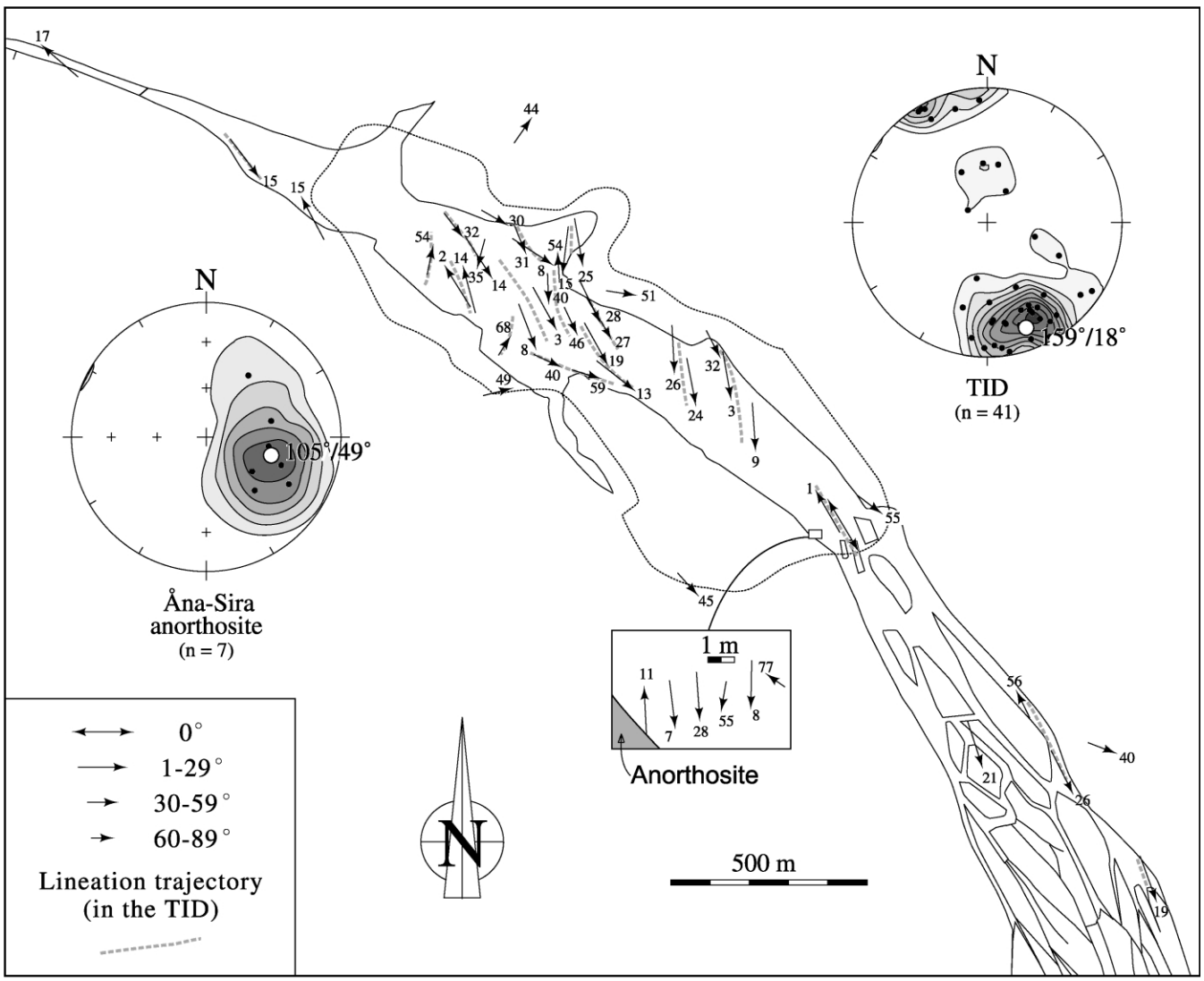

Fig. 8. Map of the magnetic lineations (K_1 axes), with Schmidt stereo-plot (lower hemisphere) of contours of these lineations with average value for data in the TID and in the Åna–Sira anorthosite (*n*: number of measurements).

them are present (Fig. 4a); and (2) the existence in some samples of symplectitic magnetite resulting from olivine destabilization, which increases the primary magnetite content of the rock and, therefore, its bulk magnetic susceptibility.

The AMS strength and shape have been expressed using, respectively, the P' and T parameters (Jelinek, 1981):

$$P' = \exp\sqrt{2\left[\left(\ln\frac{K_1}{K_m}\right)^2+\left(\ln\frac{K_2}{K_m}\right)^2+\left(\ln\frac{K_3}{K_m}\right)^2\right]}$$

and

$$T = \frac{2(\ln K_2 - \ln K_3)}{\ln K_1 - \ln K_3} - 1$$

In the samples from the Åna–Sira anorthosite, P' varies between 1.10 and 1.32 (Table 2), with a mean value of 1.19, and in the TID, values of P' range from 1.01 (almost spherical AMS ellipsoid) to 1.25 (Table 2), with an average of 1.11. In the main dike (T38), the AMS ellipsoid is weakly anisotropic ($P' = 1.05$). Whatever the provenance of the samples (Åna–Sira anorthosite, TID or main dike), there is no correlation between P' and K_m (Fig. 6a).

As illustrated by the distribution of the data, either below or above the $T = 0$ line in a T–P' graph (Fig. 6b), both prolate ($-1 < T < 0$) and oblate ($0 < T < 1$) AMS ellipsoids are found. In the Åna–Sira anorthosite, T ranges from -0.31 to 0.15 (Table 2); In the TID, T covers a larger range of values, from -0.77 to 0.59 (Table 2). In both cases, the T mean value (-0.06 for the Åna–Sira anorthosite and 0.10 for the TID) points to a triaxial average AMS ellipsoid. In T38, from the main dike, $T = 0.16$ (slightly oblate AMS ellipsoid). Again, it is noteworthy that the T–P' plot (Fig. 6b) exhibits no correlation between anisotropy degree and shape parameter.

The lack of correlation between K_m, P', and T in the TID,

Table 3
$pAARM_{0-20}$ and $pAARM_{30-60}$ data. N as in Table 2; P' and T: anisotropy degree and shape parameters of Jelinek (1981), calculated as for AMS (see text for definition); A_1 and A_3: long and short principal axes of the $pAARM_{0-20}$ ellipsoid; Dec. and Inc., s_1 and s_2 as in Table 2

Site #	N		P'	T	A_1				A_3			
					Dec.	Inc.	s_1	s_2	Dec.	Inc.	s_1	s_2
		ARM_{0-20} (A/m)										
T5	5	5.05	1.26	−0.10	334	11	66	11	229	53	70	27
T14	5	15.52	1.39	−0.41	189	21	24	11	32	67	86	8
T19	5	15.94	1.27	−0.60	175	17	6	2	27	70	73	4
T29	4	22.67	1.42	−0.05	96	71	25	5	193	2	13	1
T31	6	16.77	1.28	−0.29	160	42	43	25	322	46	53	19
T36	4	0.73	1.32	−0.78	55	10	46	39	265	79	125	22
T38	4	15.84	2.47	0.32	310	9	32	11	43	16	31	6
T42	4	5.43	1.68	0.54	163	32	57	19	257	6	34	4
		ARM_{30-60} (A/m)										
T5	5	0.29	1.27	0.53	18	28	98	22	283	9	32	18
T14	5	0.57	1.45	−0.11	197	18	30	18	84	51	40	19
T19	5	1.05	1.05	0.61	302	15	99	37	200	38	52	12
T29	4	1.36	1.19	−0.06	60	71	40	8	178	10	34	29
T31	6	0.86	1.12	−0.30	163	66	63	21	280	12	41	36
T36	4	0.18	1.22	0.38	220	74	85	12	126	1	27	5
T38	4	0.13	1.26	0.06	329	17	49	23	64	16	52	23
T42	4	0.26	1.11	−0.25	11	52	31	6	271	7	78	10

as well as the wide range of T values and also the absence of any conspicuous evolution of all these scalar parameters across the orebody in map view (not shown), probably reflect the heterogeneity of the magnetic mineralogy.

4.2. Principal directions

In the anorthosite enclosing the TID, the magnetic foliation (i.e. the $\{K_1\ K_2\}$ plane, perpendicular to the K_3 direction) tend to strike along NNW–SSE with moderate dipping (Fig. 7). This foliation pattern is roughly in accordance with the planar structures (mineral foliations and compositional layering) mapped by Krause et al. (1985) to the NE of the Åna–Sira dome top (Fig. 2a). Magnetic lineations (K_1 directions) in the anorthosite have a relatively homogeneous orientation, with calculated average 105°/49° (Fig. 8).

In the studied portion of the TID, most magnetic foliations along the orebody contacts tend to be parallel to these contact (Fig. 7). The magnetic foliations are N–S- to NW–SE-striking, usually with ENE to NE moderate (30°–59°) to steep (≧60°) dips near the SW flank, and WSW to SW moderate dips near the NE flank. A progressive rotation of the magnetic foliation pattern towards a major apophysis, is locally observed. Sites sampled far from the contacts have magnetic foliations which strike oblique or perpendicular to the orebody NW–SE-trending axis and that gently dip (≤29°) dominantly to the SE. It is concluded from the above considerations that the magnetic foliation pattern observed in the open-pit mimics the 3D shape of the TID in that area (a SE-plunging elongated trough whose NE and SW flanks dip SW and NE, respectively, and which presents some apophyses) (Fig. 2a and b). In the horsetail splay-shaped network of dikes connected to the SE dike-like tip of the orebody, magnetic foliations strike NNW–SSE, and dip steeply NE.

Magnetic lineations in the TID (Fig. 8) are N–S- to NW–SE-trending and most of them are S-to-SE-plunging with gentle to moderate values. Magnetic lineations with northern plunges are mainly found along the SW flank of the orebody. Deflection of the relatively homogeneous magnetic lineation pattern occurs, as it is the case for the magnetic foliation one, towards the major apophysis of the NE flank. The calculated mean magnetic lineation is 159°/18° (Fig. 8), an orientation strikingly similar to that of the magnetic foliation best axis, i.e. 156°/16° (Fig. 7). This points to a 155–160/15°–20° for the orientation of the TID axis.

In order to assess the magnetic fabric behavior at the contact with the host rock, a short cross-section was made at the south-eastern end of average 155°–160° strike, 15°–20° plunge to the open-pit (T49 and T44–T48; Fig. 2a), running from the SW flank of the TID (T49 and T44) up to 5 m inside the mineralization (T48). The observed magnetic fabrics are in agreement with the above described pattern (Figs. 7 and 8), even if the magnetic foliations are slightly oblique compared with the orientation of the TID contact in that area. Their strike is relatively constant from site to site although their dip evolves from moderate to steep values. The plunge values of the magnetic lineation varies from gentle to moderate. In the easternmost site (T48) magnetic foliation and lineation departs from this relatively homogenous pattern (Figs. 7 and 8). This peculiar orientation is due to the location of T48 close to the reverse ductile fault

which cuts across the orebody in that area and has induced a strong solid-state deformation, locally mylonitic in the ore.

In the main dike (T38), magnetic foliation and lineation are orientated 137°/71° (i.e. the strike is sub-parallel to the dike direction) and 311°/17°, respectively (Table 2; Figs. 7 and 8).

5. Significance of the magnetic fabric and the petrofabric

5.1. Contribution from anisotropy of partial anhysteretic remanence

A study of the pAARM was conducted on rock cylinders from the few sites previously characterized by coercivity measurements. The pAARM of the two magnetite fractions that were discriminated on the coercivity spectra (Fig. 4a and b). Large (low-coercivity) and small (medium-coercivity) grains, were determined by measurements from 0 to 20 mT ($pAARM_{0-20}$) and from 30 to 60 mT ($pAARM_{30-60}$), respectively (see Appendix A for methodology). The results of $pAARM_{0-20}$ and $pAARM_{30-60}$ measurements are shown in Table 3.

For sites T5, 29, 31, 42 (from the TID) and T38 (from the main dike), the $pAARM_{0-20}$ is strikingly coaxial with AMS (Fig. 9). Since AMS represents an average fabric, weighted according to the intrinsic magnetic susceptibility and anisotropy of the dia-, para- and ferromagnetic rock forming minerals (e.g. Jackson, 1991; Borradaile and Henry, 1997). Since $pAARM_{0-20}$ is due here to large (low-coercivity) magnetite grains, this coaxiality demonstrates that AMS is dominated by the large magnetite grains. Recent studies (Grégoire et al., 1998; Launeau and Cruden, 1998; Arbaret et al., 2002) have shown that such magnetic fabrics are mainly controlled by the shape-preferred orientation (SPO) of the magnetite grains (Uyeda et al., 1963), rather than by magnetic interactions between magnetite grains (distribution anisotropy; Hargraves et al., 1991). Accordingly, the sites for which coaxiality between ASM and $pAARM_{0-20}$ is obvious have very similar ellipsoid shapes, as evidenced by their T parameters (Tables 2 and 3).

For sites T14 (from the TID), and site T36 (from the Åna–Sira anorthosite), $pAARM_{0-20}$ is distinctly more prolate ($T < -0.40$) when compared with AMS (Tables 2 and 3), and the principal axes of the two fabrics are slightly (T14) or strongly (T36) oblique (Fig. 9). This does not preclude, however, that AMS is dominated by large magnetite grains. The 0–20 mT window covers a relatively large range of magnetite grain sizes (from some tens to several hundreds of micrometers), as deduced both petrographically and from magnetite coercivity vs. grain size data (Jackson et al., 1988; Vlag et al., 1996). In such lithologies with different magnetite grain sizes, AMS is mainly controlled by the coarser-grained fraction whereas AARM is dominated by the finer particles (e.g. Dunlop and Özdemir, 1997). Therefore, the differences in orientation and shape between $pAARM_{0-20}$ and AMS for T14 and T36 possibly results from a strong control of the $pAARM_{0-20}$ by elongated magnetite grains belonging to the smallest fraction (some tens of micrometers) of the 0–20 mT window. In the case of T14, the negligible obliquity between AMS and the prolate finer-grained magnetite suggest that the latter have a primary (igneous) origin. It can therefore be concluded that in most sites, AMS is dominated by the SPO of the coarser-grained magnetite fraction, even where such grains are in trace amounts and were not optically detected (as exemplified by site T5).

For sites T29 (TID) and T38 (main dike), the $pAARM_{30-60}$ can be considered as coaxial with the $pAARM_{0-20}$ (and hence the AMS) (Fig. 9). Since, in addition, T parameters of the $pAARM_{30-60}$ have values similar to those of the $pAARM_{0-20}$ and AMS (Tables 2 and 3), it is obvious for both sites that the $pAARM_{30-60}$ is controlled by fine-grained, medium-coercivity magnetites of primary origin, coeval with the coarse-grained fraction.

For sites T5, T42 (TID), and T36 (anorthosite) the $pAARM_{30-60}$ is distinctly oblique to both the $pAARM_{0-20}$ and the AMS (Fig. 9). Positive T values (>0.35) for the $pAARM_{30-60}$ of T5 and T36 (Table 3) suggest a medium-coercivity magnetite fraction dominated by oblate grains (possibly micro-fractures filled with magnetite, as it has been suggested elsewhere in a more detailed study of the fabric of the small-grained magnetites in the TID; Trindade et al., 2001). Similarly, a negative T value (-0.25) for the $pAARM_{30-60}$ of T42 (Table 3) suggests a strong control by fine-grained prolate magnetites (needle-like magnetite inclusions in plagioclase?). For T14 and T31 (TID), orientation of the $pAARM_{30-60}$ is slightly different from the $pAARM_{0-20}$ and AMS (except for the long principal axis) (Fig. 9).

5.2. Microtextures in the TID

Petrographically, our samples from the TID (Fig. 3) have a subophitic texture defined by euhedral crystals of plagioclase (laths with 1 to 4–5 aspect ratio), orthopyroxene, and subordinate olivine.

The euhedral and interstitial grains of plagioclase, orthopyroxene and olivine can be interpreted as minerals that crystallized at the liquidus and from interstitial trapped liquid, respectively (cumulus versus intercumulus status). In other respects, the plagioclase and orthopyroxene laths locally show a common SPO, which confers a planar fabric to the rock (Fig. 3a and b). This mineral foliation results either from a flow process during emplacement of the TID (accepting the model of sorted cumulates injected as a crystal mush; Wilmart et al., 1989) or from an in-situ crystallization process (Krause et al., 1985). The plagioclase and orthopyroxene prismatic crystals locally show evidence of heterogeneously distributed high-T solid-state deformation at the thin section scale and from one sample to another; this feature includes bending, ondulatory extinction

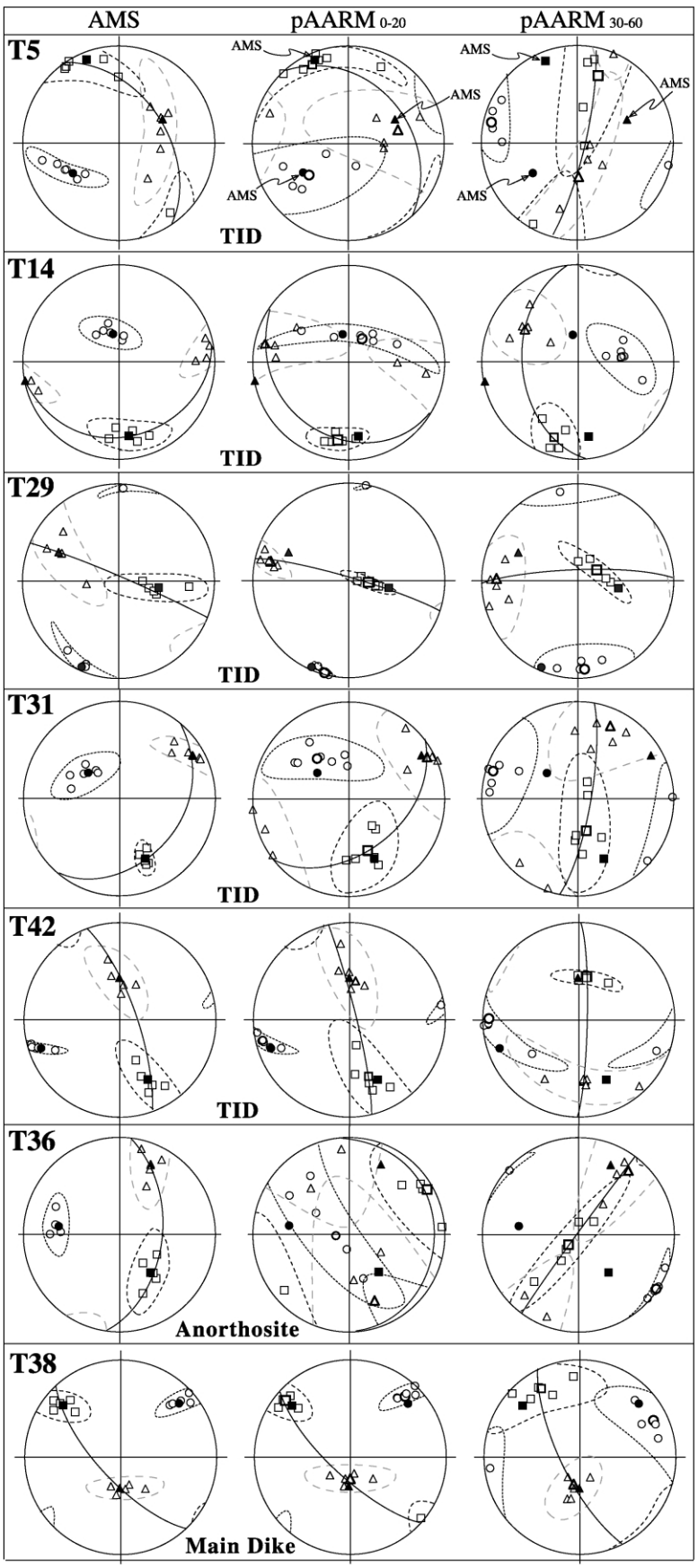
AMS
pAARM 0-20
pAARM 30-60
T5
AMS
AMS
AMS
AMS
AMS
AMS
TID
T14
TID
T29
TID
T31
TID
T42
TID
T36
Anorthosite
T38
Main Dike

and deformation twins (in plagioclase), kinking (in bronzite), and local dynamic recrystallization into aggregates of small grains (both minerals). The presence of unstrained interstitial minerals between these strained liquidus crystals indicates that solid-state deformation operated in the presence of interstitial liquid, i.e. in the sub-magmatic state (Paterson et al., 1989; Bouchez et al., 1992). These microtextures, as well as the absence of any conspicuous field evidence of in-situ crystal accumulation (such as modal layering), support the sorted cumulate model of Wilmart et al. (1989).

The frequent interstitial habit of ilmenite with regard to the euhedral silicates does not mean that this Ti–Fe oxide crystallized from a late-liquid. On the contrary, ilmenite is a liquidus mineral that started crystallizing before the euhedral plagioclase, orthopyroxene and olivine crystals, as evidenced by inclusions of isometric ilmenite grains in the silicates (Fig. 3a, b and d). The liquidus character of ilmenite being a direct consequence of the high Fe–Ti content of the magma (Duchesne, 1996, 1999). Most ilmenite grains, however, crystallized with a sub-spherical shape and smaller dimensions than the prismatic silicates. They formed together with the silicates and accumulated with them in the interstices between the larger silicate crystals. Coalescence of grains by subsolidus grain boundary readjustment (Hunter, 1996), possibly enhanced by syn-emplacement deformation in the crystal mush, has locally produced larger ilmenite areas molding around the contours of the euhedral crystals. Subsolidus reequilibration between ilmenite and magnetite, as evidenced mainly by reaction rim of spinelliferous ilmenite, have also possibly led to some grain boundary readjustments. Thus accumulation and recrystallisation of the oxides produced a structure which is a kind of 'negative' image of the plagioclase and orthopyroxene lath subfabric (Fig. 3a–c). The opaque subfabric therefore mimics the primary petrofabric of the ore, which is mainly defined by the common SPO of the plagioclase and orthopyroxene prismatic crystals.

5.3. Contribution from image analysis

Coaxiality between magnetic fabric and petrofabric was tested by an IA investigation of the opaque subfabric, taken to be representative of the petrofabric, on 20 samples from the TID and T38 from the main dike. Given the complex morphology of the opaque subfabric, the intercept method of Launeau and Robin (1996) (see http://www.sciences.univ-nantes.fr/geol/UMR6112/index.html), based on an analysis of the boundary orientation distribution of objects (obtained in filtering and thresholding the numeric images digitized using a color CCD mounted on a binocular, 5 × magnification and a rotating polarizer stage of Fueten (1997), http://craton.geol.brocku.ca/faculty/ff/ff1.html), was chosen for this study, rather than the inertia shape tensor method, based on an averaging of orientation and shape parameter of each object.

For each selected AMS site, IA was applied on three thin sections cut parallel to the K_1K_2, K_2K_3 and K_1K_3 planes, respectively, from a hand-size oriented sample. Output of the IA is a 3D quadratic shape tensor (Shimamoto and Ikeda, 1976), representative of the opaque subfabric SPO (see Fig. 10a for methodology). It is noteworthy that characterization of the petrofabric through this IA technique results from a long chain of actions, from the field sampling to the 3D reconstruction, each of them causing and propagating errors. On the contrary, the AMS technique is a more efficient and less time-consuming method based on a direct 3D determination. This justifies its use to picture the internal structure of the TID, while IA was applied only to control the reliability of the magnetic fabric.

Comparison of the IA data with the AMS results reveals an angular departure between K_1 and A, and K_3 and C, the respective long and short axes of the IA and AMS ellipsoids, that is usually less than 30°, except for T12, T14 and T27 which exhibit a larger angular difference between K_1 and A (Fig. 10b). The larger discrepancy between K_1 and A observed for these three sites possibly finds its origin in the scattering of the individual K_1 measurements in the average magnetic foliation plane, while the eight measurements of A are well grouped around the average long axis of the IA ellipsoid. The above considerations imply that magnetic fabric in the TID and the main dike can be equated to the opaque subfabric, and hence to the petrofabric, in a first approximation. Moreover, since the magnetic fabric is dominated by the coarse-grained magnetite fraction and the opaque SPO essentially outlines the ilmenite-rich areas in the TID, the IA results show that the coarse-grained magnetites have the same SPO as the ilmenites. This confirms that AMS is mainly controlled by the SPO of the coarse-grained magnetites and suggests that the grain boundary readjustments between oxides did not significantly affect the magnetite primary SPO.

6. Discussion

Poles to magnetic foliations and magnetic lineations in the Åna–Sira anorthosite near the TID show an average NW–SE strike and NE moderate dip and E–W direction

Fig. 9. Schmidt stereo-plots (lower hemispheres) of AMS, $pAARM_{0-20}$ and $pAARM_{30-60}$ for AMS sites characterized by pAARM measurements. Open symbols: ellipsoid principal axes of individual specimens (square, long axis; triangle, intermediate axis; circle, short axis); Same symbols, heavy: average of the individual axes; dotted lines around the axis distribution: 3σ (standard error) confidence ellipse. The average principal axes of the AMS ellipsoid are represented for comparison in the $pAARM_{0-20}$ and $pAARM_{30-60}$ stereo-plots.

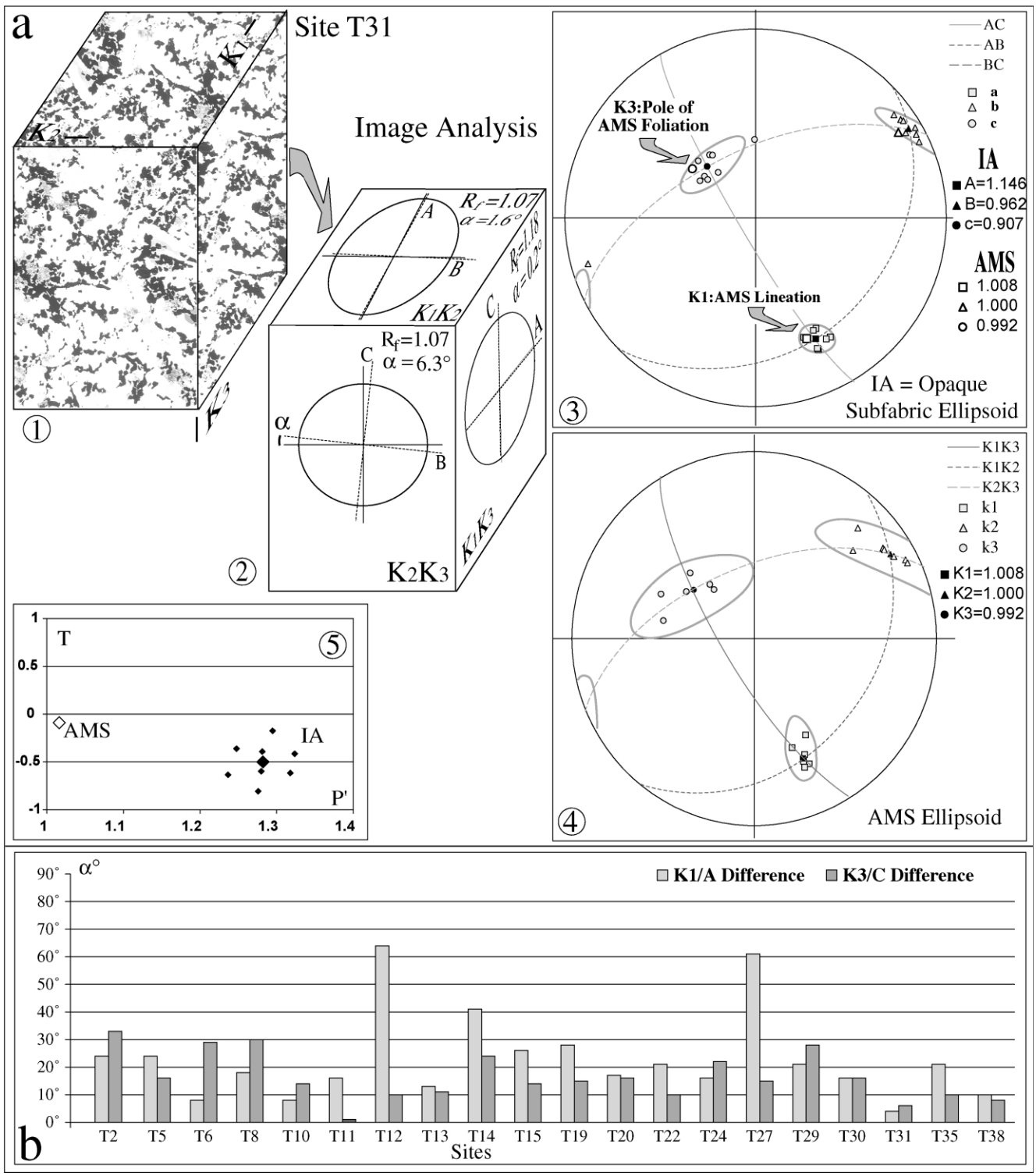

Fig. 10. (a) IA analytical procedure, exemplified for site T31: (1) filtering and thresholding of three digitized image (dimensions: ~1.4 mm × 1.9 mm) of thin sections cut parallel to the K_1K_2, K_2K_3 and K_1K_3 planes, respectively, in order to optically isolate the subfabric of the opaque grains; (2) quantification of the opaque subfabric (intercept method of Launeau and Robin, 1996); α is the angular departure between the principal axes of the 2D shape tensor and the corresponding axes of the AMS ellipsoid in the section. R_f is the shape ratio; (3) combination of the three pairs of 2D quadratic shape tensors yields an ellipsoid representative of the 3D SPO of the opaque grains. Individual axes of the eight combinations, their average and 3σ (standard error) confidence ellipse are represented in the lower hemisphere of a Schmidt stereo-plot and compared with the AMS ellipsoid principal axes. (4) AMS data for T31 site for comparison; (5) plot of AMS and IA shape parameter (T) vs. anisotropy degree (P'); (b) Angular departure between the long and short principal axes of the AMS and IA ellipsoids, respectively.

with E moderate plunge, respectively. Correlation of these structures with the anorthosite petrofabric was not assessed here, although a rough parallelism between magnetic foliations and planar structures measured in the field (mineral foliations and compositional layering) exists (Figs. 2a and 7). Also, the pattern of the magnetic lineations is in agreement with theoretical predictions of stretching lineations in a diapiric dome (Cruden, 1990) for this part of the anorthositic body. A detailed interpretation of the AMS data from the Åna–Sira anorthosite is beyond the scope of this paper. It is, however, noteworthy that the average magnetic fabric depicted in this pluton is oblique to the TID one (Figs. 7 and 8). This obliquity is especially obvious for the magnetic lineations. Together with the sharp contact and the brittle deformation (incipient cleavage) evidenced in the anorthosite and the TID, it constitutes an additional argument in favor of an emplacement of the TID after complete crystallization of the enclosing anorthosite. This assessment is consistent with that previously established by field studies (Krause and Pedall, 1980; Krause et al., 1985) and geochronology (Schärer et al., 1996).

In the TID, parallelism of the magnetic foliation trajectories with the contacts indicates that the magmatic petrofabric is acquired in a magma flow rather than resulting from in-situ crystallization during accumulation. Local fuzzy layering is here the result of transposition of an inhomogeneous magma in the foliation during emplacement of the TID. The homogeneity of the magnetic lineation pattern, from the SE horsetail splay-shaped network of dikes to the NW end of the TID, also argues in favor of a flow-inherited fabric. Thus, AMS measurements, combined with microtextural evidence of deformation in the sub-magmatic state and field evidence for lack of in-situ crystal accumulation, strongly support the idea that the TID emplaced in the form of a crystal mush (e.g. Wilmart et al., 1989).

The SSE to NNW lateral spreading of the crystal-mush along the average N159°/18° direction of the lineation is evidenced by: (1) the deflections of the foliation/lineation near the apophysis and especially near the north one where the clockwise trend of the lineation draw the flow from SSE toward NNE; (2) the local obliquity between magnetic foliation/lineation and the direction of the western orebody wall. (Figs. 7 and 8 and enlargement of the Southern contact from sites 44 to 49 near the south-western wall). Accordingly, the feeding-zone of the TID is probably located to the south-east of the orebody below the horsetail splay-shaped network of dikes. Crystal-mush batches were progressively intruded from this region and injected towards the NNW.

The enrichment mechanism in Ti–Fe oxides envisaged by Wilmart et al. (1989) is a gravity segregation process, which would have led to a stratification of the postulated magma chamber, with a noritic cumulate, enriched in dense Ti–Fe minerals, at the bottom and another one, enriched in light plagioclases, at the top. Draining of this zoned magma chamber would have first yielded injection of the plagioclase-rich part of the cumulates (now found along the contact of the TID, in its southeastern and northwestern ends, and in apophyses), followed by the ilmenite-rich part (now forming the main portion of the orebody). An amount of 3 to 10% of intercumulus melt, lubricating the sorted cumulate at the time of emplacement, was calculated in this model.

Åreback and Stigh (2000) have recently described an ilmenite-rich leuconorite layered body whose mineralogy and geochemistry are strikingly similar to that of the TID in the central part of the Neoproterozoic Hakefjorden noritic complex (southwestern Sweden). This ilmenite-rich layered body is interpreted as intruding a batch of plagioclase and Ti–Fe oxide-laden liquid (Åreback and Stigh, 2000). Its strong enrichment in Ti and Fe resulted from a continuous fractionation of a residual noritic magma, which left after crystallization of anorthosite at depth and that rose up to intermediate depth to form the Hakefjorden noritic complex (Ashwal, 1993). Strong enrichment in iron and titanium is characteristic for residual liquids left after anorthosite crystallization (Emslie et al., 1994; McLelland et al., 1994).

The similarity of initial Sr isotopic compositions between the TID and the Rogaland anorthosite bodies (Wilmart et al., 1989) is also a good argument in favor of a noritic parental magma for the TID. Residual from the crystallization of the Åna–Sira anorthosite, or at least of an hidden similar pluton, given that a time gap of ~10 Myr (Schärer et al., 1996) separates the TID and its host rock crystallization. Thus, the ilmenite-rich layered body described by Åreback and Stigh (2000) may be a good example of the magma chamber which injected the TID. Preliminary melting experiments conducted on ilmenite norite from the TID suggest a jotunite-like intercumulus melt at the pressure (5 kbar) of emplacement of the TID (Skjerlie et al., 2001). These results implicitly confirm the jotunitic composition assumed by Wilmart et al. (1989) in their calculation of the amount of trapped liquid. Hence, a jotunitic parental magma is to be envisaged for the layered body presumably connected to the TID. Such a liquid is not a residual product of anorthosite crystallization: on the contrary, it is similar but slightly evolved in composition to the anorthosite parental magma (Longhi et al., 1999). A jotunitic parent also substantiates the analogies in mineral composition that are observed (Duchesne and Schiellerup, 2001) between the TID and some cumulate units of the neighboring Bjerkreim–Sokndal intrusion, which crystallized from a jotunitic parental magma (Vander Auwera and Longhi, 1994). The Bjerkreim–Sokndal intrusion is too large, and also probably too old, to be the feeder of the TID. A layered body similar in size to the small Hogstad lens (not dated), outcropping in the Åna–Sira anorthosite, 10 km to the southeast of the TID, which has a jotunitic parental magma (Vander Auwera and Duchesne, 1996), would be a better candidate.

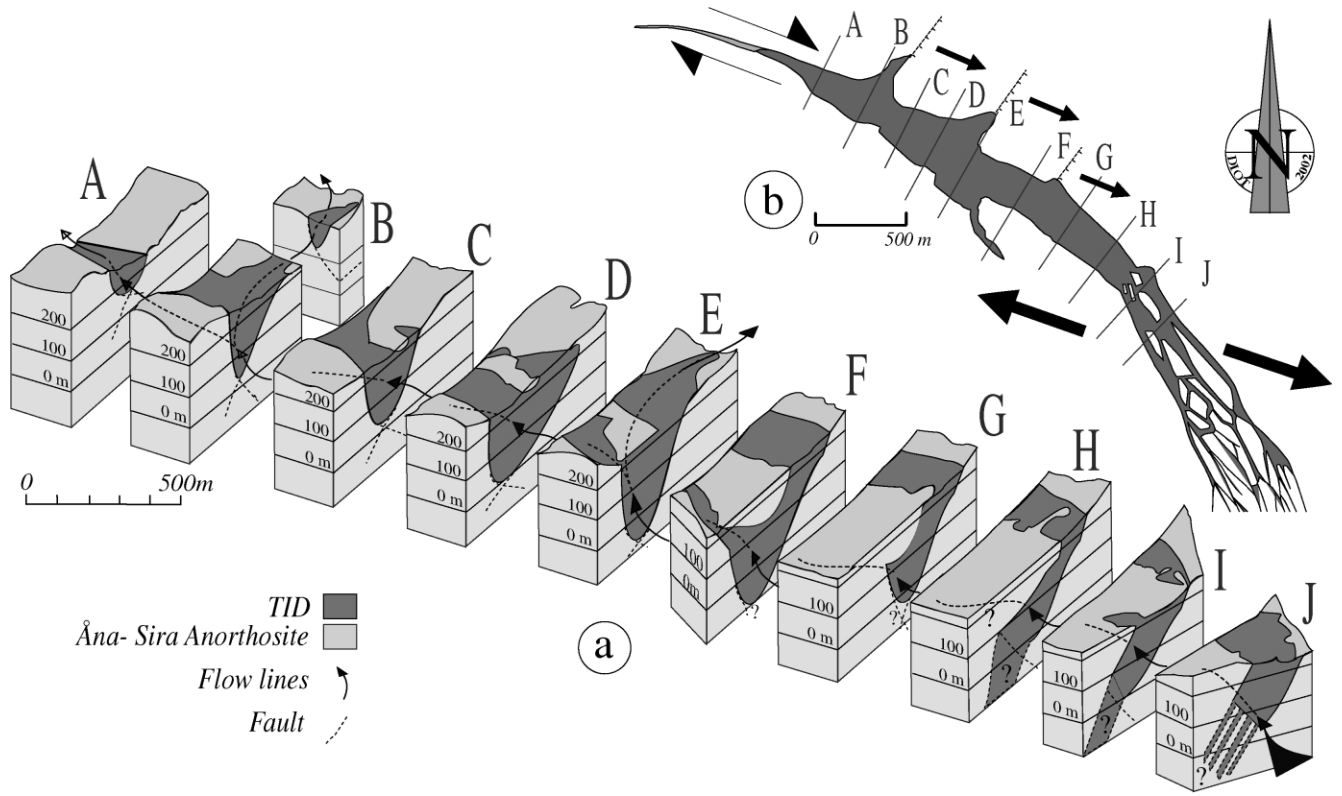

Fig. 11. (a) 3D view of the TID (Titania A/S document, pers. comm., 1999) with superposed average flow lines in the crystal mush during its emplacement, deduced from the magnetic lineation pattern. The 3D block of the TID used in the representation has been reconstructed from microgravimetric data, conducted prior to the beginning of the orebody working, which explains why contacts are significantly different from today. (b) Tectonic model proposed for emplacement of the TID, with location of profiles A to J of (a).

7. Conclusion

We propose an emplacement of the TID by coalescence of batches of noritic crystal-rich mush whose petrofabric was acquired during syn-emplacement deformation. The sub-magmatic flow related with this emplacement is determined by an AMS study checked by pAARM measurements, IA investigation and petrographical observations. The average orientation of this flow is given, in a first approximation, by the mean magnetic lineation, i.e. 159/18°.

In agreement with the model of Wilmart et al. (1989), the crystal-mush is a noritic cumulate escaped from an unknown magma chamber and injected in the TID. The weakness zone that triggered the emplacement of the TID has been active for at least 10 Myr, allowing the emplacement of successive non-comagmatic magma batches in a single geological unit. First the several-kilometer-long main dike was intruded at 931 ± 5 Ma. Later the small dikes of the jotunitic kindred were intruded. These small dikes have not been dated but locally crosscut the Tellnes main dike and therefore are younger than 931 Ma. Finally, at 920 ± 3 Ma, the TID was emplaced.

The sickle-shaped outcrop of the TID further suggests that injection of the crystal mush from the southeastern NNW–SSE-striking feeding-zone, was favored by the transcurrent, dextral opening of a WNW–ESE-striking (N120°) weakness-zone across the Åna–Sira anorthosite (Fig. 11b). The opening of the apophyses, along the NE flank of the orebody, can be explained by a transfer, along ENE–WSW normal faults, of part of the dextral relative movement between the SW and NE sides of the N120° weakness-zone (Fig. 11b). The emplacement scenario proposed for the TID, i.e. the dextral-opening of a sphenochasm, calls for a local extensional faulting environment into which the magma pressure has certainly contributed to the initiation of fractures in the differential regional stress. Emplacement of noritic crystal-mush batches into a sphenochasm in the Åna–Sira anorthosite, provides an elegant mechanism for its draining.

Acknowledgments

The authors wish to thank K. Berge and R. Hagen from Titania A/S for their hospitality at the Tellnes mine, for valuable discussion and encouragement during this work, and also for providing unpublished information concerning the TID. Field work and part of the AMS and IA studies were financially supported by Titania A/S, who also authorized the publication of the results. Comments by Jeff Gee, Basil Tikoff and Cat Walter contributed to the

improvement of the manuscript. pAARM measurements were made by O.B. under the supervision of R. Trindade during a post-doctoral stay at the Paul-Sabatier University (Toulouse, France).

Appendix A. Methodology

A.1. Measurements of coercivity spectra

AMS represent a contribution of all rock-forming minerals (dia-, para- and ferromagnetic). ARM (anisotropy of remanent magnetization) is given exclusively by ferromagnetic minerals of various grain size and the partial anhysteretic remanence (pARM) is correlate with the grain size (Jackson et al., 1988). The following procedure was used for coercivity determinations: AF demagnetization in 100 mT, to establish the background remanent magnetization (i.e. the residual remanence linked to high-coercivity minerals), followed by successive cycles, from $H = 10$ to 90, of AF magnetization at H mT (with a superimposed DC field of 0.05 mT applied by a small coil inside and coaxial to the demagnetizer), AF demagnetization at $H - 10$ mT and pARM determination. AF magnetizations and demagnetizations were made in a LDA3-AMU1 apparatus (Agico Ltd) into which demagnetization is performed on rotating rock specimens (in order to minimize the gyro-remanence effect which could arise from very small magnetite grains; Stephenson, 1993). DC field was controlled by a Molspin apparatus. A JR5A spinner magnetometer (Agico Ltd) (sensitivity $< 100\ \mu A/m$) was used for the pARM measurements.

A.2. Measurements of AMS

AMS measurements were performed on a Minisep spinner susceptometer (Molspin Ltd) which works in a weak alternative field (7×10^{-4} T, 10 kHz) with a sensitivity of $\sim 5 \times 10^{-7}$ SI. Some results, for specimens with low AMS and/or low magnetic susceptibility, were checked on a Kappabridge susceptometer KLY-2 (Agico Ltd) (working values 3.8×10^{-4} T, 875 Hz; sensitivity 2×10^{-8} SI). Differences between outcomes from the two instruments did not exceed a few percent.

Measurements provided, for each rock cylinder, the length of the three principal, mutually orthogonal axes of the AMS ellipsoid ($K_1 \geqq K_2 \geqq K_3$), and their orientation (trend and plunge) with respect to the specimen frame. For each sampling site, the averages of the principal axis lengths and orientations in the geographical frame were calculated from the rock cylinders (three to six specimens per site) following the tensor averaging method of Hext (1963) (P. Launeau software).

A.3. Measurements of pAARM

The chosen measurement procedure consists of successive pARM acquisitions and determinations along six positions of the rock specimen. In this scheme, two successive positions are symmetrical, which allows elimination of the background remanent magnetization (established by AF demagnetization in 100 mT before pARM acquisition for each position pair). Following the procedure proposed by Trindade et al. (2001), ARM was acquired by applying an AF field of 20 mT (with a DC field of 0.05 mT) for $pAARM_{0-20}$ measurements. Specimens were AF magnetized at 60 mT (with a DC field of 0.05 mT), before being AF demagnetized at 30 mT, for $pAARM_{30-60}$ measurements. AF magnetizations and demagnetizations and pAARM measurements were made, respectively, on the LDA3-AMU1 demagnetizer and the JR5A spinner magnetometer (Agico Ltd). As for AMS, the average lengths and orientations of the pAARM ellipsoid principal axes ($A_1 \geqq A_2 \geqq A_3$) were calculated, for each studied site, from measurements on the rock cylinders, using the tensor averaging method of Hext (1963) (P. Launeau software). For specimens with low pAARM degree and/or low ARM intensity, three to four pAARM determinations were conducted, and their average was calculated before being introduced in the mean pAARM ellipsoid calculation.

References

Arbaret, L., Launeau, P., Diot, H., 2002. Significance of magnetic and three-dimensional Shape Preferred Orientation of magnetite in simple shear flow. Tectonophysics, in press.

Åreback, H., Stigh, S., 2000. The nature and origin of an anorthositic associated ilmenite-rich leuconorite, Hakefjorden Complex, south-west Sweden. Lithos 51, 247–267.

Ashwal, L.D., 1993. Anorthosites, Springer-Verlag, Heidelberg, 422pp.

Barnichon, J.D., Havenith, H., Hoffer, B., Charlier, R., Jongmans, D., Duchesne, J.C., 1999. The deformation of the Egersund–Ogna anorthosite massif, south Norway: finite-element modeling of diapirism. Tectonophysics 303, 109–130.

Bingen, B., Demaiffe, D., van Breemen, O., 1998. The 616-My-old Egersund basaltic dike swarm, SW Norway, and late Proterozoic opening of the Iapetus Ocean. The Journal of Geology 106, 565–574.

Bolle, O., Diot, H., Duchesne, J.C., 2000. Magnetic fabric and deformation in charnockitic igneous rocks of the Bjerkreim–Sokndal layered intrusion (Rogaland, Southwest Norway). Journal of Structural Geology 22, 647–667.

Borradaile, G.J., Henry, B., 1997. Tectonic applications of magnetic susceptibility and its anisotropy. Earth-Science Reviews 42, 49–93.

Bouchez, J.L., 1997. Granite is never isotropic: an introduction to AMS studies of granitic rocks. In: Bouchez, J.L., Hutton, D.H.W., Stephens, W.E. (Eds.), Granite: From Segregation of Melts to Emplacement Fabric, Kluwer, Dordrecht, pp. 95–112.

Bouchez, J.L., Delas, C., Gleizes, G., Nedelec, A., Cuney, M., 1992. Submagmatic micro-fractures in granites. Geology 20 (1), 35–38.

Cruden, A.R., 1990. Flow and fabric development during the diapiric uprise of magma. Journal of Geology 98, 681–698.

Delaney, P.T., Pollard, D.D., Ziony, J.I., McKee, E.H., 1986. Field relations between dikes and joints: emplacement processes and paleostress analysis. Journal of Geophysical Research 91, 4920–4938.

Duchesne, J.C., 1973. Les gisements d'oxydes de fer et de titane dans les roches anorthositiques du Rogaland (Norvège méridionale). In: Morin, P., (Ed.), Les roches plutoniques dans leurs rapports avec les gÎtes minéraux, Masson, Paris, pp. 241–248.

Duchesne, J.C., 1996. Liquid ilmenite or liquidus ilmenite: a comment on the nature of ilmenite vein deposits. In: Demaiffe, D., (Ed.), Petrology and Geochemistry of Magmatic Suites of Rocks in the Continental and Oceanic Crusts, Université Libre de Bruxelles-Royal Museum for Central Africa (Tervuren), pp. 73–81.

Duchesne, J.C., 1999. Fe–Ti deposits in Rogaland anorthosites (South Norway): geochemical characteristics and problems of interpretation. Mineralium Deposita 34, 182–198.

Duchesne, J.C., Schiellerup, H., 2001. The iron-titanium deposits. In: Duchesne, J.C. (Ed.), The Rogaland Intrusive Massifs: an Excursion Guide. Norges geologiske undersøkelse Report 2001.029, pp. 57–78.

Duchesne, J.C., Maquil, R., Demaiffe, D., 1985. The Rogaland anorthosites: facts and speculations. In: Tobi, A.C., Touret, J.L.R. (Eds.), The Deep Proterozoic Crust in the North Atlantic Provinces, Reidel, Dordrecht, pp. 449–476.

Duchesne, J.C., Liégeois, J.P., Vander Auwera, J., Longhi, J., 1999. The crustal tongue melting model and the origin of massive anorthosites. Terra Nova 11, 100–105.

Dunlop, D.J., Özdemir, O., 1997. Rock Magnetism: Fundamentals and Frontiers, Cambridge University Press, Cambridge, 573pp.

Emslie, R.F., Hamilton, M.A., Thiérault, R.J., 1994. Petrogenesis of a Mid-Proterozoic Anorthosite–Mangerite–Charnockite–Granite (AMCG) complex: isotopic and chemical evidence from the Nain Plutonic Suite. Journal of Geology 102, 539–558.

Falkum, T., Petersen, J.S., 1980. The Sveconorwegian orogenic belt, a case of Late-Proterozoic plate-collision. Geologische Rundschau 69, 622–647.

Force, E.R., 1991. Geology of titanium mineral deposits. Geological Society of America Special Paper 259, 118.

Fueten, F., 1997. A computer controlled rotating polarizer stage for the petrographic microscope. Computers and Geosciences 23, 203–208.

Gierth, E., 1970. Die Ilmenitlagerstätte Tellnes (Süd-Norwegen). Ph.D. Thesis, T.U. Clausthal.

Gierth, E., Krause, H., 1973. Die Ilmenitlagerstätte Tellnes (Süd-Norwegen). Norsk Geologisk Tidsskrift, Supplement 53, 359–402.

Gierth, E., Krause, H., Schott, W., 1982. Paragenesen und Gefüge des hydrothermalen Nachhalls in südnorwegischen Titaneisenerzen. Erzmetall 35, 441–446.

Grégoire, V., Darrozes, J., Gaillot, P., Nédélec, A., Launeau, P., 1998. Magnetite grain shape fabric and distribution anisotropy vs. rock magnetic fabric: a three-dimensional case study. Journal of Structural Geology 7, 937–944.

Hargraves, R.B., Johnson, D., Chan, C.W., 1991. Distribution anisotropy: the cause of AMS in igneous rocks? Geophysical Research Letters 18, 2193–2196.

Hext, G.R., 1963. The estimation of second-order tensors, with related tests and design. Biometrika 50, 353–373.

Hoagland, R.G., Hahn, G.T., Rosenfield, A.R., 1973. Influence of microstructure on fracture propagation in rock. Rock Mechanics 5, 77–106.

Hunter, R.H., 1996. Texture development in cumulate rocks. In: Cawthorn, R.G., (Ed.), Layered Intrusions, Development in Petrology 15, Elsevier, Amsterdam, pp. 77–101.

Jackson, M., 1991. Anisotropy of magnetic remanence: a brief review of mineralogical sources, physical origins, and geological applications, and comparison with susceptibility anisotropy. Pure Applied Geophysics 136, 1–28.

Jackson, M., Gruber, W., Marvin, J., Banerjee, S.K., 1988. Partial anhysteretic remanence and its anisotropy: applications and grainsize-dependence. Geophysical Research Letters 15, 440–443.

Jelinek, V., 1981. Characterization of the magnetic fabrics of rocks. Tectonophysics 79, 63–67.

Karlsen, T.A., Nilsson, L.P., Marker, M., Gautneb, H., Erichsen, E., 1998. Berggrunnsgeologi og mineralske ressurser i Sokndals-området, Rogaland. Norges geologiske undersøkelse Report, 98068.

Krause, H., Pedall, K.G., 1980. Fe–Ti mineralizations in the Åna–Sira anorthosite, Southern Norway. In: Siivola, J. (Ed.), Metallogeny of the Baltic Shield. Finland Geological Survey Bulletin 307, pp. 56–83.

Krause, H., Gierth, E., Schott, W., 1985. Ti–Fe deposits in the South Rogaland igneous complex with special reference to the Åna–Sira anorthosite massif. Norges geologiske undersøkelse Bulletin 402, 25–37.

Lagroix, F., Borradaile, G.J., 2000. Magnetic fabric interpretation complicated by inclusions in mafic silicates. Tectonophysics 325, 207–225.

Launeau, P., Robin, P.Y.F., 1996. Fabric analysis using the intercept method. Tectonophysics 267, 91–119.

Launeau, P., Cruden, A.R., 1998. Magmatic fabric acquisition mechanisms in a syenite: results of a combined anisotropy of magnetic susceptibility and image analysis study. Journal of Geophysical Research 103, 5067–5089.

Longhi, J., Vander Auwera, J., Fram, M.S., Duchesne, J.C., 1999. Some phase equilibrium constraints on the origin of Proterozoic (massif) anorthosites and related rocks. Journal of Petrology 40, 339–362.

McLelland, J., Ashwal, L.D., Moore, L., 1994. Composition and petrogenesis of oxide-, apatite-rich gabbronorites associated with Proterozoic anorthosite massifs: example of the Adirondack mountains, New York. Contribution to Mineralogy and Petrology 116, 225–238.

Paterson, S.R., Vernon, R.H., Tobisch, O.T., 1989. A review of criteria for the identification of magmatic and tectonic foliations in granitoids. Journal of Structural Geology 11, 349–363.

Pollard, D.D., 1973. Derivation and evaluation of a mechanical model for sheet intrusions. Tectonophysics 19, 233–269.

Rochette, P., 1987. Magnetic susceptibility of the rock matrix related to magnetic fabric studies. Journal of Structural Geology 9, 1015–1020.

Rochette, P., Jackson, M., Aubourg, C., 1992. Rock magnetism and the interpretation of the anisotropy of magnetic susceptibility. Reviews of Geophysics 30, 209–226.

Schärer, U., Wilmart, E., Duchesne, J.C., 1996. The short duration and anorogenic character of anorthosite magmatism: U–Pb dating of the Rogaland Complex, Norway. Earth and Planetary Science Letters 139, 335–350.

Shimamoto, T., Ikeda, Y., 1976. A simple algebric method for strain estimation from deformed ellipsoidal objects. 1. Basic theory. Tectonophysics 36, 315–337.

Skjerlie, K.P., Kullerud, K., Robins, B., 2001. Preliminary melting experiments on the Tellnes ilmenite norite from 0.5 to 1.2 GPa, implications for the composition of intercumulus melt (abstract). In: Korneliussen, A. (Ed.), Abstracts—GEODE Field Workshop 8–12th July 2001 on Ilmenite Deposits in the Rogaland Anorthosite Province, S. Norway. Norges geologiske undersøkelse Report 2001.042, pp. 135–136.

Smithson, S.B., Ramberg, I.B., 1979. Gravity interpretation of the Egersund anorthosite complex, Norway: its petrological and geothermal significance. Geological Society of America Bulletin 90, 199–204.

Stephenson, A., 1993. Three-axis static alternating field demagnetization of rocks and the identification of natural remanent magnetization, gyroremanent magnetization, and anisotropy. Journal of Geophysical Research 98, 373–381.

Streckeisen, A., 1974. How should charnockitic rocks be named? In: Duchesne, J.C., Bellière, J. (Eds.), Géologie des domaines cristallins, Volume du Centenaire de la Société Géologique de Belgique, Liège, pp. 349–360.

Trindade, R.I.F., Bouchez, J.L., Bolle, O., Nédélec, A., Peschler, A., Poitrasson, F., 2001. Secondary fabrics revealed by remanence anisotropy: methodological analysis and examples from plutonic rocks. Geophysical Journal International 147, 310–318.

Uyeda, S., Fuller, M.D., Belsch, J.C., Girdler, R.W., 1963. Anisotropy of magnetic susceptibility of rocks and minerals. Journal of Geophysical Research 68, 279–291.

Vander Auwera, J., Duchesne, J.C., 1996. Petrology and geochemistry of the noritic Hogstad layered body (Rogaland, southwestern Norway): evidence for a jotunitic parent magma. In: Demaiffe, D., (Ed.), Petrology and Geochemistry of Magmatic Suites of Rocks in the Continental and Oceanic Crusts, U.L.B.-Royal Museum for Central Africa (Tervuren), pp. 111–127.

Vander Auwera, J., Longhi, J., 1994. Experimental study of a jotunite (hypersthene monzodiorite): constraints on the parent magma composition and crystallization conditions (P, T, fO_2) of the Bjerkreim–Sokndal intrusion (Norway). Contributions to Mineralogy and Petrology 118, 60–78.

Vlag, P., Rochette, P., Dekkers, M.J., 1996. Some additional hysteresis parameters for a natural (titano)magnetite with known grain size. Geophysical Research Letters 23, 2803–2806.

Wilmart, E., Demaiffe, D., Duchesne, J.C., 1989. Geochemical constraints on the genesis of the Tellnes ilmenite deposit, Southwest Norway. Economic Geology 84, 1047–1056.